AD

USAAVLABS TECHNICAL REPORT 67-49

REDUCTION OF HAZARD FROM SECONDARY FRAGMENTS CREATED BY BALLISTIC PENETRATION OF AIRCRAFT

By

R. F. Recht
W. G. Newell

October 1967

U. S. ARMY AVIATION MATERIEL LABORATORIES
FORT EUSTIS, VIRGINIA

CONTRACT DA 44-177-AMC-399(T)
DENVER RESEARCH INSTITUTE
UNIVERSITY OF DENVER
DENVER, COLORADO

DEPARTMENT OF THE ARMY
U S ARMY AVIATION MATERIEL LABORATORIES
FORT EUSTIS, VIRGINIA 23604

The technical objective of this contract was the design, test, and evaluation of a suppressant system capable of reducing the volume and lethality of spall and debris resulting from penetration of aircraft by small-arms projectiles.

The material and the means of application presented in this report are possible approaches to the problem. However, the use of the recommended system to restrict structural spall would require penalties that are not considered to be acceptable by present operational aircraft.

The analyses and techniques reported herein are sound, and the results may be considered as background information in future studies and design objectives. However, this command does not concur with the proposed suppressant system for installation on the UH-1 aircraft because the technique is not considered to be practical.

This report is published for the dissemination of information, for the stimulation of discussion, and for use as a guideline in further efforts to investigate this particular problem of optimization of a suppressant design.

Task 1F121401A15003
Contract DA 44-177-AMC-399(T)
USAAVLABS Technical Report 67-49
October 1967

REDUCTION OF HAZARD FROM SECONDARY FRAGMENTS CREATED BY BALLISTIC PENETRATION OF AIRCRAFT

REPORT NUMBER 931-6702-F

by

R. F. Recht
W. G. Howell

Prepared by

Mechanics Division
Denver Research Institute
University of Denver
Denver, Colorado

for

U. S. ARMY AVIATION MATERIEL LABORATORIES
FORT EUSTIS, VIRGINIA

ABSTRACT

The objective of this research effort was to establish a practical means of alleviating the hazard to personnel within occupied areas of Army aircraft due to secondary projectiles (spall and debris) created by ballistic impact of aircraft structure and equipment by small-arms projectiles. The characteristics of secondary fragments generated by ballistic penetration of typical aircraft structural materials were established for a variety of impact conditions. The impact conditions which created the greatest hazard to personnel due to secondary fragments were used to evaluate suppressant systems designed to reduce or eliminate this hazard. A suppressant system was developed which proved to be capable of stopping virtually all secondary fragments generated by impact of structural materials tested.

TABLE OF CONTENTS

TABLE OF CONTENTS (Cont.)

LIST OF ILLUSTRATIONS

LIST OF ILLUSTRATIONS (Cont.)

LIST OF ILLUSTRATIONS (Cont.)

LIST OF TABLES

LIST OF SYMBOLS

V_0 - initial velocity of the projectile, ft/sec

V_{rp} - residual velocity of the projectile, ft/sec

V_{rf} - velocity of secondary fragment, ft/sec

V_{rfn} - velocity of secondary fragment having a trajectory parallel to initial projectile trajectory ($\beta = 0$), ft/sec

V_x - minimum perforation velocity, ft/sec

θ - angle* of impact obliquity (measured between projectile trajectory and normal to the target at the point of impact; this angle lies in horizontal plane)

ϕ - projectile yaw angle* (measured between projectile axis and projectile trajectory; this angle lies in horizontal plane)

β - angle* between secondary fragment trajectory and initial projectile trajectory ($\tan \beta = \frac{r}{D_0}$)

D_0 - normal distance between impact point and witness, inches

D_{0p} - normal distance between impact point and pattern witness, inches

r - radial distance measured on witness between fragment perforation and initial projectile trajectory intercept

x - horizontal component of r

y - vertical component of r

β_x - angle* between projection of secondary fragment trajectory on horizontal plane and initial projectile trajectory ($\tan \beta_x = x/D_0$)

---

* These angles are considered to be positive when measured clockwise.

LIST OF SYMBOLS (Cont.)

$\beta_{x\gamma}$ - $\beta_x - \gamma$

β_y - angle between projection of secondary fragment trajectory on verticle plane (containing initial projectile trajectory) and initial projectile trajectory ($\tan \beta_y = y/D_0$)

β'_x - $\arctan \frac{r^2}{xD_0} = \arctan \frac{r}{D_0} \left(1 \Big/ \sqrt{1 - (\frac{y}{r})^2} \right) = \arctan \frac{\tan^2 \beta}{\tan \beta_x}$

$\beta'_{x\gamma}$ - angle related to β'_x and γ (see text)

α_{xL}, α_{xR}, α_{yU}, α_{yD}
- angles defining limits of beam spray pattern; measured from the original trajectory to the left and right horizontal limits (x) and up and down vertical limits (y)

d - projectile caliber, in.

L_p - equivalent length of projectile assumed to be a cylinder of diameter, d, in.

L - length of rectangular fragment, in.

W - width of rectangular fragment, in.

T - thickness of rectangular fragment, in.

γ - angle* given by $\gamma = \frac{\theta + \phi \pm 90°}{2}$ ($\pm$ is positive when ϕ is negative; is negative when ϕ is positive)

W_p - weight of projectile, grains

W_f - weight of fragment, grains

W_{f0} - total weight of fragments driven from plate, grains

M - total mass of a piece of material, $\frac{\text{lb-sec}^2}{\text{in.}}$

LIST OF SYMBOLS (Cont.)

w - specific weight of target material, grains per cubic inch

ρ - mass density, $\frac{\text{lb-sec}^2}{\text{in.}^4}$

U - stress wave velocity in a material (in./sec)

C - sound wave velocity in a material (in./sec)

σ - tensile stress, psi

ϵ - tensile strain (in./in.)

τ - shear stress, psi

c - small c used as a subscript indicates a critical value of the parameter

ψ - constant related to impact impedance

Δ - AP - Single plate (Al)

$\blacktriangle$ - AP - Double plate (Al)

$\blacktriangle$ - AP - Casting (Al)

$\bigcirc$ - Ball - Single plate (Al)

$\bullet$ - Ball - Double plate (Al)

$\bigcirc$ - Ball - Casting (Al)

I. INTRODUCTION

The primary objective of the research reported herein was to establish a practical means of alleviating the hazard to personnel within occupied areas of Army aircraft due to secondary projectiles (spall and debris) created by ballistic impact of aircraft structure and equipment by small arms projectiles. To achieve this objective, the program was conducted in two semi-concurrent phases outlined below:

Phase I. Experimental determination of physical and dynamic characteristics of fragments generated when typical aircraft materials were impacted by yawing caliber .30 projectiles. Specific conditions for impact were as follows:

> Projectiles: caliber .30 AP M2 and caliber .30 ball M2
> Impact Velocities: 1500 and 2500 feet per second
> Target Obliquities: 0 and 45 degrees (CCW from above)
> Projectile Yaw at Impact: 45 and 90 degrees (CW) and 45 degrees (CCW)

The materials and equipment which were impacted in accordance with the above criteria are listed in Section III.

Test results, summarized in Appendix II, were analyzed to determine the repeatability and predictability of impact test results and to determine the impact conditions which create fragments presenting the greatest hazard to personnel.

Phase II. Selection and development of suppressant systems capable of eliminating the hazard due to secondary fragments. These suppressant systems were evaluated under those impact conditions determined in Phase I to be most hazardous to personnel.

The experimental procedures employed and the results of the program are discussed in following sections.

II. EQUIPMENT AND EXPERIMENTAL TECHNIQUES

2.1 PROJECTILE LAUNCH TECHNIQUE

Several methods for obtaining the specified projectile yaw angles were considered; the simplest and most straightforward was tried first and proved to be reliable. The projectiles were fired from a smoothbore gun (0.308-inch bore) having an asymmetrical geometry at the muzzle; i.e., a muzzle attachment was used which had a stepped exit, as shown in Figures 1 and 2. As the projectile emerged, the propellant gases were released more rapidly on one side of the projectile and a lateral force was applied to its base. Since the projectile was not spin-stabilized, it yawed quite freely in response to this lateral force. There was also a slight tendency for the projectile to pitch when launched in this manner. A series of tests was conducted to determine the yaw rates and the repeatability when this launch technique was used for two projectiles at specified velocities; the four-channel Model 730 Fexitron X-ray system was used, as schematically illustrated in Figure 3. The yaw and pitch rates for a given projectile and velocity were found to be constant and repeatable; thus, the yaw angle at impact could be predetermined by controlling the distance from muzzle to target. The pitch attitude at impact was corrected to zero degrees for each distance by angular adjustment of the muzzle attachment.

2.2 EQUIPMENT AND PROCEDURES

The basic arrangement for conduct of the experimental program is shown schematically in Figure 4. A target chamber was constructed in which the target, witness screens, velocity switches, etc., could be maintained with fixed distance relationships to one another. The fragment velocity witness was divided into 36 zones, 16 of which could be instrumented with velocity switches in any one test. Continuous, conductive-printed-circuit, ballistic tape was used for velocity switches to determine time of flight for projectile and fragments; a typical setup for a test is illustrated in Figure 5. The velocity switch circuits were connected to a multiple-channel, time-measurement system. The time of flight of the projectile between velocity switches 1 and 2 was recorded on a counter providing data for determination of projectile velocity (see Figure 4). When the circuit for switch 2 was broken, a type 555 oscilloscope received a start signal, and each

circuit broken thereafter by projectile or fragments produced a signal which was characteristic of the particular zone in which the switch was located. These signals were recorded on the oscilloscope; a typical Polaroid oscilloscope record is presented in Figure 6. From this record, time of flight of the fastest fragment to cut the circuit in each zone was obtained for velocity determination. Data reduction procedures are discussed in Section III, and further discussion of the instrumentation is presented in Appendix I. Other special equipment used to provide further insight into dynamics of secondary fragments included high-speed photographic and X-radiographic equipment. Some of the tests were covered by a Model WF-3 Fastax camera running at approximately 7000 frames per second. Other tests were covered by a Model 326 Dynafax camera operating at 25,000 frames per second.

III. SECONDARY FRAGMENTS GENERATED DURING NORMAL AND OBLIQUE BALLISTIC IMPACT OF PLATE GEOMETRIES BY YAWING PROJECTILES

Secondary fragments, generated when projectiles impact target components, represent an additional threat to components and personnel. To design suppressant systems to defeat this threat, or to account for secondary fragment effects during vulnerability studies, it is necessary to define the threat in sufficient detail for such purposes. Yawing caliber .30 armor-piercing and ball projectiles were fired (impact velocities: 2500 and 1500 feet per second) at single and double, rolled, metal plate geometries, cast alloy plates, transparent plates, wire bundles, and various aircraft components (nominal plate thicknesses: 2024 T3 aluminum single plates - 0.025, 0.040, 0.063 inch; cast aluminum and magnesium alloys - 0.125, 0.025 inch). The experiments were designed to determine secondary fragment patterns (spray angles) and the typical characteristics of individual fragments in terms of (1) their weights and shapes, (2) their trajectories, and (3) their velocities.

As the definition of the secondary fragment threat emerged from the experimental program, design criteria for the development of suppressant systems were formulated. These criteria can be used to guide the development of design concepts into effective, efficient, and practical suppressants capable of defeating specific secondary fragment threats. Since suppressant systems are not armor systems and, thus, are not designed to defeat the primary projectile, they should perturb the projectile as little as possible.

3.1 DEFINITION OF SECONDARY FRAGMENT THREAT

An objective of the experimental program was to define the dynamics of secondary fragments generated when a projectile strikes and perforates specified target materials and items. Information gained from the experiments was utilized to define, quantitatively, the threat represented by such secondary fragments. It served as a basis for evaluating suppressant concepts aimed at defeating the threat.

When an overmatching projectile encounters a target, it may pass on through intact or it may break up (portions of its jacket may be stripped off and the core may break). The ballistic impact will generate

secondary fragments composed of target materials. Impact velocity, obliquity, and projectile yaw will each influence the characteristics of projectile breakup and secondary fragment generation. To properly define the threat associated with a specified projectile-target encounter, it is necessary to determine the weight, shape, velocity, and direction of the major fragments, as well as the beam-spray angles which establish the boundaries of affected zones behind the target. Experimental results have been correlated empirically, and a predictive equation for secondary fragment velocity has been developed. The data on aluminum rolled plates and aluminum cast plates were used to develop empirical and analytical relationships. These relationships serve to correlate the data for cast magnesium plates and to provide a basis for comparisons with data obtained on glass and Plexiglas plate materials, as well as tubing and wire bundles. Consequently, the development of empirical and analytical relationships pertaining to aluminum rolled and cast plates precedes the consideration of other materials in this report.

The following indicates the scope of the experimental program:

Projectiles:	caliber .30 armor-piercing (AP-M2) and caliber .30 ball (M/2)
Target Materials:	Plate (rolled and cast aluminum, cast magnesium, glass, safety glass, Plexiglas) Steel tubing Wire bundles Flight instruments
Impact Velocities:	2500 and 1500 feet per second
Impact Obliquities:	0 and 45 degrees (CCW)
Projectile Yaw:	45 and 90 degrees (CW) and 45 degrees (CCW)

3.2 EXPERIMENTAL PROCEDURES AND DATA REDUCTION

The symbols defined on page xi are used consistently throughout this discussion. Figure 7 illustrates the means by which the required measurements are made. The plan view shows the projectile moving toward the target with a velocity, V_0, along a trajectory which encounters the target at an obliquity, 0. Obliquity is measured between the trajectory and the normal to the target. (Since the plate and its normal

are rotated counterclockwise, the illustrated obliquity is defined as θ (CCW).) As depicted, the projectile is yawed counterclockwise in the plane of the plan view at an angle, ϕ. As the projectile passes through the target, it is deflected slightly to the right and downward from its initial trajectory, impacting at B. Secondary fragments encounter the pattern witness within the dashed rectangle shown on the front elevation view. The beam spray angle, α_X, defines the width of the rectangle (X_L plus X_R) for a given value of D_{0p}; the angles α_L and α_R sum to αX and locate the vertical edges of the rectangle. Angles αY, α_U and αD define the height of the rectangle (Y_U plus Y_D) and locate the horizontal edges in a similar manner.

For ease of illustration, only one major fragment (identified as F) is shown on the plan view. The times required for major fragments to traverse the distance between target impact and the velocity witness are measured using break screens; the flight distances are measured so that fragment velocity, V_{rf}, can be determined. A fragment velocity can be measured for each of the zones (16 shown) which make up the velocity witness. Major fragments are those for which weight is recorded. A rectangle defined by the four maximum values of x and y (or β_X and β_Y) associated with the major fragments can be used to establish beam-spray information pertaining to the major fragments. The direction of major fragments is established by measuring x and y displacements from a reference point on the witness (this reference point is defined by the intercept of the pre-impact trajectory of the projectile with the witness). The radius, r, is also measured. These measurements are used with the normal distance, D_0, to determine the angular relationships between the pre-impact trajectory of the projectile and the direction taken by a fragment. The angle between these two lines is identified by β; its tangent is r/D_0. The projections of the fragment trajectory on the x and y planes are defined by angles β_X and β_Y whose respective tangents are x/D_0 and y/D_0.

If a standard constant normal distance is maintained between the impact point and the pattern witness, lengths measured on the witness are directly related to angles, and fragment patterns can be compared directly. Direct comparison of fragment patterns is especially useful when suppressant materials are being evaluated; effects of a suppressant on patterns are directly observable. A normal distance, D_0, of approximately 11 inches was used.

Two types of rectangles are used to define the limits of fragment spray patterns. Those which define the limits of the total pattern include all fragment impacts arbitrarily. Those which define the limits of the major fragment pattern include all major fragment impacts (fragments whose weights are recorded) arbitrarily. Judgement is not required to determine rectangles in this manner. Several rectangles related to a given geometry are compared, and a more typical rectangle is obtained by including within it those areas which are common to the majority.

A standard data reduction sheet, completed as shown in Figure 8, was used to record and reduce experimental data. Each completed sheet is a formal representation of the test results. Information in the upper right-hand corner describes the pre-impact geometry of the test. The target is described in the upper left-hand corner. Post-impact conditions pertaining to the projectile follow. A record was made of the zones which sustain fragment impact; the approximate number of fragment impacts in each zone was noted. That zone which contained the reference point defined by the pre-impact trajectory intercept was listed first. The velocity witness provided a measurement of time of flight for the fastest fragment which succeeded in breaking the printed circuit in each zone. These velocities were recorded as being typical of fragment velocities in each zone. Major recovered fragments were weighed. Their dimensions were recorded, as well as their shape, to establish typical fragment geometries. Measurements of x, y, and r were made, and angles were determined. Beam-spray angles were determined from the pattern witness and listed on the sheet.

High-speed photography and flash X-rays were used to obtain detailed information concerning the dynamics of secondary fragments and the perforating projectile. Figure 9 illustrates the nature of the secondary fragment problem. This Dynafax high-speed photographic series records the post-impact dynamics associated with oblique perforation of a 0.188-inch cast aluminum plate by a yawed ball projectile (Test No. 237: impact obliquity, projectile yaw, and projectile velocity were 45 degrees CCW, 90 degrees CW, and 2500 feet per second respectively). The orthogonal flash X-ray photographs, reproduced on Figure 10, illustrate the fragment pattern 272 microseconds after perforation of a similar cast aluminum plate at zero obliquity (AP-M2 projectile yaw and velocity were 90 degrees and 2530 feet per second, respectively). The horizontal (plan) view is parallel to the plane in which obliquity and yaw angles are measured; the vertical (elevation) view is parallel to the plane containing the vertical axis of rotation about which angles

are measured (see Figure 7). Symmetry should be observed in the vertical view. These results typify secondary fragment dynamics for cast materials and other materials which are characteristically susceptible to brittle fracture. Ductile materials produce fewer fragments, but dispersion patterns and velocities are similar. Note that certain fragments possess higher velocities than the residual velocity of the projectile. Patterns as projected on planes tend to be elliptic and, in many cases, nearly circular. Circular patterns would indicate that fragment velocity is directly proportional to the cosine of the direction angle, β, defined as the angle between the fragment trajectory and the initial trajectory of the projectile. Note that the initial trajectory does not bisect the pattern in Figure 9; the direction of maximum fragment velocity is not generally observed to coincide with the initial projectile trajectory. Consequently, an angle, γ, which defines the direction of maximum fragment velocity, must be defined when attempting to predict fragment velocity, V_{rf} (in any direction), as a function of maximum fragment velocity, V_{rfn}. Assuming that patterns are spherical leads to the following predictive equation for the ratio of fragment velocity in any direction to the maximum fragment velocity

$$\frac{V_{rf}}{V_{rfn}} = \cos \gamma \cos(\beta - \gamma) \qquad (1)$$

To be useful, both the maximum fragment velocity, V_{rfn}, and its direction defined by β must be established either empirically or analytically. Also, it has been observed that pattern projections tend to be circular in the plan view and elliptic in the elevation view. Consequently, the equation requires additional modification to account for fragments which have directions defined by β_y as well as β_x. In any direction, fragment velocities vary below the highest fragment velocities associated with that direction. The velocity attributed to fragments impacting a particular zone on the witness during a given test was that of the first fragment to reach the zone and break the circuit. Consequently, velocity prediction equations relate to such fragments (these highest velocities are undoubtedly the most consistent).

3.3 SECONDARY FRAGMENT VELOCITIES

An adequate definition of maximum fragment velocity, V_{rfn}, is required to develop Equation (1) into a useful form. The residual velocity of a projectile which perforates a thin plate is closely predicted by[1]:*

$$V_{rp} = \frac{1}{1 + \frac{W_{f0}}{W_p}} \sqrt{V_0^2 - V_x^2} \tag{2}$$

where W_{f0} (the total fragment weight) is the weight of plate material removed

V_x is the minimum perforation velocity (protection ballistic limit)

The target geometries considered are easily perforated by the caliber .30 projectiles, even at high obliquity and yaw, the minimum perforation velocity rarely exceeding 500 feet per second. The lowest projectile velocity of 1500 feet per second is at least three times as great. Inspection of Equation (2) reveals that when the impact velocity, V_0, is more than three times as great as the minimum perforation velocity, the influence of V_x on the residual velocity of the projectile is less than 6 percent. Consequently, the residual velocity of the projectile is predicted closely by the following relationship, provided that $V_0 >> V_x$:

$$V_{rp} = \frac{1}{1 + \frac{W_{f0}}{W_p}} V_0 \tag{3}$$

The total weight of the secondary fragments, W_{f0}, driven from the plate can be closely approximated by using the projected outline of the projectile on the surface of the plate, projection lines being parallel to the direction of motion. The area enclosed by this outline multiplied by the plate thickness and specific weight provides a value for W_{f0}. This results in the following equation for the weight ratio required in Equation (3):

$$\frac{W_{f0}}{W_p} = \frac{w\ Td\ (L_p \sin \phi + \frac{\pi d}{4} \cos \phi)}{W_p \cos \theta} \tag{4}$$

* Superscripts refer to listed References.

For the caliber .30 armor-piercing projectile, Equation (4) reduces to:

$$\frac{W_{f0}}{W_p} = \frac{(11.6 \sin \phi + 3.0 \cos \phi)\, wT}{7000 \cos \theta} \qquad (5)$$

where T is plate thickness in inches

w is specific weight of target material in grains per cubic inch.

Equation (5) can also be used to represent values associated with the caliber .30 ball projectile. It yields the same value of the ratio at ϕ = 90 degrees and gives values only 1.5 percent and 6 percent (maximum deviation) low at 45 degrees and 0 degrees, respectively. Since yaw values of interest were either 90 degrees or 45 degrees, Equation (5) was used for both projectiles. Substituting Equation (5) into Equation (3) gives an expression which closely predicts residual velocity of the projectile, provided that $V_0 >> V_x$.

A projectile yawed at 90 degrees in the horizontal plane which impacts a plate at zero obliquity will tend to drive fragments along trajectories lying in the vertical plane containing the initial projectile trajectory. The maximum fragment velocity will be maximum along the initial projectile trajectory. This observation derives from considerations of symmetry and is illustrated by Figure 10. It is obvious that this maximum velocity cannot be less than the residual velocity of the projectile, since the maximum velocity direction is coincident with the direction of the projectile. Consequently, the projectile residual velocity given by Equation (3) serves as a lower bound on the maximum secondary fragment velocity.

Secondary fragments commonly attain velocities greater than the residual velocity of the projectile, often exceeding the projectile's initial impact velocity, V_0. The maximum velocity that a fragment could have can be accurately defined by considering the coplanar impact of two plates. A target plate is initially stationary and is impacted by a flyer plate made of the same material as the projectile. This situation is that used to study the solid state Hugoniot behavior of materials[2, 3]. The impact pressure at the coplanar interface is given by:

$$p = \frac{\rho_2 U_2 V_0}{1 + \frac{\rho_2 U_2}{\rho_1 U_1}} \qquad (6)$$

where p is impact pressure, psi

ρ is mass density, $\frac{\text{lb sec}^2}{\text{in.}^4}$

U is Hugoniot wave velocity, in./sec ($\cong \sqrt{\frac{K}{\rho}}$, where K is bulk modulus)

V_0 is initial velocity, in./sec

1 and 2 are subscripts representing the flyer plate (projectile) and target plate, respectively

This pressure accelerates the target material to:

$$V_2 = \frac{2\,V_0}{1 + \frac{\rho_2 U_2}{\rho_1 U_1}} \tag{7}$$

provided that $\frac{T_1}{U_1} \geq \frac{T_2}{U_2}$ (where T is plate thickness)

Considering again the impact geometry characterized by zero obliquity and 90 degrees yaw, Equation (7) should represent the maximum velocity of a fragment driven from a very thin plate, since as thickness approaches zero, the coplanar impact condition is approached. However, the lateral surface of the projectile is circular; consequently, the coplanar impact with the very thin plate is represented by Equation (7) only along an impact line. If plate fragments are very small, Equation (7) should predict the velocities of fragments originating near this "line" impact. Fragments driven from the plate, which were initially remote from the impact line, will have lower velocities. The velocity component parallel to the direction of the projectile should be approximately $V_2 \cos \alpha$ where V_2 is given by Equation (7) and α is the angle between the projectile trajectory and the radial line to the point of impact (from the projectile axis). If the material driven from the plate remains intact (a single fragment), its velocity is obtained by integrating $V_2 \cos \alpha$ from $\alpha = 0$ to $\alpha = 1$ radian (i.e., the fragment width is approximately equal to the projectile caliber). If this is done, its velocity is given by:

$$V_2 = \frac{1.68\,V_0}{1 + \frac{\rho_2 U_2}{\rho_1 U_1}} \tag{8}$$

Equations (7) and (8) can be used to represent brittle and ductile materials respectively (i.e., brittle materials which degenerate into a great many fragments will produce maximum velocities greater than will ductile materials which produce fewer fragments).

As target plates become thicker, the coplanar plate impact no longer represents the situation. Observations show that as thickness increases, the fragment velocity tends to approach the residual velocity of the projectile[1].

When T = 0, the residual velocity of the projectile is equal to the initial velocity. For this case, the difference between fragment velocity and projectile residual velocity is maximum and is the difference between Equation (7) or (8) and V_0. If this difference decays exponentially with increasing thickness, its value is given by:

$$\Delta V = (V_2 - V_0)\, e^{-C\,T/d} \tag{9}$$

$$\text{or } \Delta V \quad \psi\, V_0\, e^{-C\,T/d} \tag{10}$$

where $\psi = \dfrac{2}{1 + \dfrac{\rho_2 U_2}{\rho_1 U_1}}$ -1.0 for brittle target materials

or

$= \dfrac{1.68}{1 + \dfrac{\rho_2 U_2}{\rho_1 U_1}}$ -1.0 for ductile target materials

Maximum fragment velocity, V_{rfn}, is equal to the residual velocity of the projectile plus the difference in velocity given by Equation (9) when the maximum fragment velocity is along the projectile's initial trajectory; thus:

$$V_{rfn} = V_{rp} + \Delta V \tag{11}$$

Substituting Equations (3), (7) or (8), and (9) into Equation (11) yields:

$$V_{rfn} = \left[\frac{1}{1 + W_f/W_p} + \psi\, e^{-C\,T/d}\right] V_0 \tag{12}$$

Table I contains values of ψ for certain materials. (Values of $\rho_1 U_1$ for both projectiles (steel and lead) are equivalent, fortunately.)[3] Equation (12) concerns the maximum velocity of secondary fragments generated by a projectile yawed at 90 degrees with the trajectory (ϕ = 90 degrees) and impacting the plate at normal obliquity (θ = 0). The direction of fragments having maximum velocities is along the projectile trajectory (β_x = 0, β_y = 0).

The direction, γ, measured in the horizontal plane associated with maximum fragment velocities is a function of obliquity and yaw. This function has tentatively been represented by:

$$\gamma = \frac{\theta + \phi \pm 90^\circ}{2} \tag{13}$$

where ($\pm$) is negative when ϕ is positive (CW) and

positive when ϕ is negative (CCW)

Table II contains values of γ used during the study. Physically, this function is obtained by locating the bisector of the major angle between the plane of the plate surface and the projectile axis, and by measuring the angle, γ, between this bisector and the initial trajectory.

Thus, for fragment trajectories which lie entirely in the horizontal plane (i.e., β_y = 0) their velocity is predicted by:

$$V_{rf} = V_{rfn} \cos \gamma \cos (\beta_x - \gamma) \tag{14}$$

Equation (14) recognizes that only the component of the initial momentum (velocity) in the direction of γ contributes to the maximum fragment velocity; hence, the maximum fragment velocity associated with γ is given by $V_{rfn} \cos \gamma$. This observation is substantiated by experiments involving an obliquity of 45 degrees CCW and projectile yaw of 45 degrees CW (projectile axis parallel to plane of plate); maximum velocities are associated with a γ value of 45 degrees and are found to be about 70 percent of those associated with the θ = 0 degrees, ϕ = 90 degrees geometry used to derive V_{rfn} (Equation (12)). The angle ($\beta_x - \gamma$) relates the fragment direction to the direction of maximum fragment velocity, and its cosine is the predicted ratio of the fragment velocity to the maximum fragment velocity at $\gamma = \gamma$.

TABLE I

CONSTANTS FOR FRAGMENT VELOCITY PREDICTION EQUATION

Target Material	ψ	C
Rolled Aluminum Plate	0.18	4
Cast Aluminum Plate	0.40	2
Cast Magnesium Plate	0.60	2
Plate Glass	0.61	2
Stretched Acrylic Plastic	0.74	2

TABLE II

COMPUTED VALUES OF DIRECTION OF MAXIMUM FRAGMENT VELOCITY

Obliquity (degrees)	Yaw (degrees)	Direction of Maximum Fragment Velocity (Predicted) (degrees)
0	-45	+22.5
0	0	0
0	+45	-22.5
0	+90	0
-45	-45	0
-45	0	-22.5
-45	+45	-45
-45	+90	-22.5

Equation (14) pertains to fragments having trajectories within the horizontal plane. Secondary fragments which remain in this plane are driven from the plate much as line drives are driven from a baseball bat. Fragments which are driven upward or downward behave somewhat like pop flies or foul balls. Consequently, such fragments attain lower velocities. A study of those geometries where $\gamma = 0$ revealed that the following equation adequately predicted velocities of fragments with nonhorizontal trajectories.

$$V_{rf} = V_{rfn} \cos \beta'_x \tag{15}$$

where $$\tan \beta'_x = \frac{\tan^2 \beta_x + \tan^2 \beta_y}{\tan \beta_x} \qquad (\beta_y/\beta_x \leq 1) \tag{16}$$

Derived for any value of γ and extended to cover any ratio of β_y and β_x, Equation (16) became:

$$\tan \beta'_{x\gamma} = \frac{\tan^2 (\beta_x - \gamma) + \cos^2 \beta_x \tan^2 \beta_y}{\cos^2 (\beta_x - \gamma) \tan (\beta_x - \gamma)} \tag{17}$$

where $(\beta_y/\beta_x \leq 1)$

and

$$\tan \beta'_{x\gamma} = \frac{\tan \left(2 \arctan \frac{\cos \beta_x}{\cos (\beta_x - \gamma)} \tan \beta_y - \beta_x + \gamma\right) + \frac{\cos^2 \beta_x \tan^2 \beta_y}{\cos^2 (\beta_x - \gamma)}}{\tan \left(2 \arctan \frac{\cos \beta_x}{\cos (\beta_x - \gamma)} \tan \beta_y - \beta_x + \gamma\right)} \tag{18}$$

where $(\beta_y/\beta_x \geq 1)$

Rewriting Equation (14):

$$V_{rf} = V_{rfn} \cos \gamma \cos \beta'_{x\gamma} \tag{19}$$

Substituting Equation (12) into Equation (19) yields the general equation for secondary fragment velocity which renders Equation (1) useful for the prediction of velocities when used with Equations (5), (13), and (17) or (18).

$$V_{rf} = \left[\frac{1}{1 + W_{f0}/W_p} + e^{-C\,T/d} \right] V_0 \cos\gamma \cos\beta'_{x\gamma} \qquad (20)$$

Table I gives values for ψ and C; Table II gives values for γ; and Figures 11, 12, and 13 are plots of cos $\beta'_{x\gamma}$ (dashed line indicates the common boundary of Equations (17) and (18)).

Equation (20) predicts the velocity of a fragment which traverses a given trajectory. It does not predict direction (although γ is a good definition of the general direction taken by major fragments and the fragment cloud). It is not valid when initial projectile velocity is much less than three times the minimum perforation velocity.

Figure 14 illustrates the capability of the equation to predict experimentally measured fragment velocities. The data scatter and bias are influenced by three separate considerations:

1. Natural variations in velocity
2. Measurement error
3. Prediction error

Two high-velocity families of fragments have been observed. One is associated with the γ value given by Equation (13). The other is associated with a γ value of zero. This latter high-velocity family tends to reside in a zone close about the initial trajectory, $\beta_x < \pm 25$ degrees; it may be generated by the projectile ogive or may have another explanation. For each measured fragment, the two velocities were computed in order to classify the fragment as a member of one family or the other. *

3.4 MAJOR SECONDARY FRAGMENT SHAPE AND WEIGHT

For purposes of analysis, it is convenient and sufficient to consider fragments as being rectangular in shape. The assumption on shape reduces to the following equation for fragment weight:

---

* The velocity ratios plotted on Figure 14 were based on the following definition of the two fragment families:

When $\beta_x > \gamma$ (as computed by Equation (13)), $\gamma = \gamma$

When $\beta_x \leq \gamma$ (as computed by Equation (13)), $\gamma = 0$

Average values are shown as well as ranges of scatter.

$$W_f = L \times W \times T \times w \tag{21}$$

Secondary fragments driven from a given type of plate material would be expected to have widths, W, related to projectile caliber, and would also be expected to group into families of length to width, L/W (and, therefore, weight to thickness, W_f/T). Equation (21) can be rewritten:

$$w\ W^2 = \frac{(W_f/T)}{(L/W)} \tag{22}$$

Using this form of the equation, experimental values of W, (L/W), and $\frac{W_f}{Tw}$ are plotted for each major secondary fragment retrieved. Families are tentatively identified on the fragment weight plot, and corresponding estimates of (L/W) and (W_f/T) are assigned to each family. Adjustments are made until the typical fragments representing each family are consistently defined by both the experimental data and Equation (22). Curves defining the typical weight and shape characteristics of each fragment family as a function of yaw angle for a given target material, impact velocity, and impact obliquity are plotted.

Figures 15 and 16 present typical secondary fragment weight and shape characteristics involving caliber .30 ball and AP impacts on aluminum single plates, double plates, and cast plates. Impact geometry is depicted in the plan view at four values of yaw. An example will illustrate the means by which typical fragment characteristics are determined from the graphs. Consider AP impact of a 0.040-inch-thick aluminum plate at an impact obliquity, θ, of 45 degrees CCW and projectile yaw, ϕ, of 90 degrees CW (Figure 16). Curves 1, 4, 5, and 8 apply and, in combination, produce $\frac{W_f}{Tw}$ curves (4-8), (4-5), (1-5). While a (1-8) curve might be postulated, no fragments having such characteristics were observed. The largest typical fragment has a $\frac{W_f}{Tw}$ of 0.25 grain per inch of thickness divided by specific weight in grains per inch cubed and, therefore, weighs 6 grains. It has a width of 0.23 inch (curve 4) and a L/W ratio of 4 (curve 8); thus, its length is 0.92 inch. Similarily, the fragment which possesses a $\frac{W_f}{Tw}$ value of 0.065 has a weight of 1.8 grains, is 0.23 inch wide, and is 0.35 inch long. No fragments were specifically retrieved having (W_f/T) values of 0.02; however, such a fragment would weigh only

0.5 grain and would be 0.11 inch wide and 0.17 inch long. Many fragments of this general description are observed (only major fragments were retrieved). Cast plates produce compact fragments which characteristically possess small length to width ratios. Thus, on Figure 16 the largest cast fragment (which is observed at a yaw angle of 45 degrees CW) weighs only 0.065 grain per inch of thickness divided by specific weight as compared with the fragment driven from rolled plate by an AP projectile, which has a value of 0.25.

Symmetries and other conditions permit the construction of the curves shown in Figures 15 and 16. Spot-check experiments confirm the general validity of these curves over the entire ranges of projectile yaw.

3.5 MAJOR SECONDARY FRAGMENT DIRECTION

The diagram of the experiment shown on Figure 7 should be consulted to obtain a visual description of the angles and distances described in the following paragraphs. While it is probable that predictive equations concerning fragment direction could be developed, no concerted attempt has been made to do so. Rather, the approach has been similar to that associated with the definition of typical fragment weights and shapes. Fragment direction is obtained from the witness by measuring the radius, r, and its x and y components (r is the radial distance of the fragment from the initial projectile trajectory intercept at the witness). The total change in fragment direction from the original projectile direction is given by:

$$\beta = \arctan \frac{r}{D_0} = \arctan \sqrt{\tan^2 \beta_x + \tan^2 \beta_y} \qquad (23)$$

Projections of the angle in the horizontal and vertical planes (whose intersection is the initial projectile trajectory) are:

$$\beta_x = \arctan \frac{r}{D_0} \qquad (24)$$

$$\beta_y = \arctan \frac{y}{D_0} \qquad (25)$$

The angles β_x and β_y for each major fragment are plotted using the same graphical format used to plot weight and shape characteristics. Resulting β_x and β_y curves are identified (where possible) with weight

curves using the weight curve identification code (for example, the β_x and β_y curves associated with the (2-5) curve on Figure 15 are identified in the same manner on Figure 17).

Figures 17 and 18 present the direction angles corresponding to the fragments described on Figures 15 and 16. The β_x and β_y values pertinent to the example presented during the discussion of fragment weight and shape can be determined from Figure 18. Specific values can be obtained only for the (3-7), (4-8), and (2-6) families identified on Figure 16. Ranges of β_x and β_y are defined by β_{XL}, β_{XR}, β_{YU}, and β_{YD}. The (4-8) fragment defined in the previous example typically has a direction defined by $\beta_x = -21$ degrees and $\beta_y = \pm 3$ degrees.

For any given impact condition, the horizontal and vertical boundaries of the major fragment pattern are defined by the maximum and minimum values of x and y (associated with major fragments) and the four corresponding angles of β_x, β_y (see Figure 7). The total beam-spray angle for the horizontal and vertical directions is obtained by summing appropriate angles. This information is defined on Figures 17 and 18 by the maximum and minimum values of β_x and β_y at a given yaw angle (β_{XL}, β_{XR}, β_{YU}, β_{YD}).

The horizontal and vertical boundaries of the total fragment pattern are defined by those values of x and y which totally enclose all perforations on the witness. They are converted to the beam-spray angles defining horizontal and vertical dispersion by using the following equations:

$$(\alpha)_{XL} = \arctan \frac{X_{min}}{D_0}; \quad (\alpha)_{XR} = \arctan \frac{X_{max}}{D_0} \tag{26}$$

$$(\alpha)_{YU} = \arctan \frac{Y_{max}}{D_0}; \quad (\alpha)_{YD} = \arctan \frac{Y_{min}}{D_0} \tag{27}$$

Figures 17 and 18 also depict the beam-spray angles for the total fragment patterns corresponding to the fragments defined on Figures 15 through 18. Since the pattern is symmetrical about the x-axis, only the upper boundary as defined by $(\alpha)_{YU}$ is shown.

While no concerted attempt was made to define fragment direction analytically, it was necessary to establish a criterion for the prediction of the direction of maximum fragment velocity. As indicated in the section on secondary fragment velocities, two families of fragments

are tentatively identified. One family had a maximum velocity in the direction of the initial projectile trajectory defined as $\gamma = 0$, where γ is the angle, measured in the horizontal plane, between the initial projectile trajectory and the direction of maximum fragment velocity. The other family had a maximum velocity in a direction, measured in the horizontal plane, bisecting the major angle between the plate surface and the projectile axis at impact, so that:

$$\gamma = \frac{\theta + \phi \pm 90°}{2} \qquad (13)(28)$$

where the angles are positive when measured clockwise, and $(\pm)$ is positive when the sign on ϕ is negative, and contrariwise.

The angle γ coincides approximately with the direction of major fragments in the horizontal plane given by β_x. Consider the eight impact geometries illustrated in Figures 17 and 18. The following tabulation illustrates the correspondence between β_x for the major fragments and the angle γ as given by Equation (28).

TABLE III

COMPARISON OF β_x ANGLES ASSOCIATED WITH MAJOR FRAGMENTS AND PREDICTED VALUES OF γ

Obliquity, θ (degrees)	Yaw, ϕ (degrees)	Major Fragment Direction, β_x (Figs. 11 & 12) (degrees)	Predicted Direction of Maximum Fragment Velocities, γ (degrees)
0	-45	+25	+22.5
0	0	0	0
0	+45	-25	-22.5
0	+90	0	0
-45	-45	0 (approx.)	0
-45	0	-25 (approx.)	-22.5
-45	+45	-40	-45
-45	+90	-20	-22.5

The angle γ appears to be reasonably reliable as a means for predicting the direction of major fragments.

3.6 LOW-VELOCITY IMPACT OF ALUMINUM ROLLED AND CAST PLATES

Results obtained from tests involving projectile velocities of 1500 feet per second compare favorably with those obtained at 2500 feet per second. Fragment weights and shapes correspond, in general, to those presented on Figures 15 and 16. Their directions are correlated by the plots of Figures 17 and 18. As expected, the effect of neglecting minimum perforation velocity (see Equations (2) and (3)) is more pronounced. Fragment velocities are somewhat lower than predicted and are more erratic than those associated with fragments driven from the plates by high-velocity projectiles.

3.7 RESULTS OF EXPERIMENTS INVOLVING OTHER THAN ALUMINUM PLATE TARGETS

Cast magnesium plates yielded secondary fragments very much like those driven from cast aluminum presented on Figures 15 and 18, which can be utilized for cast magnesium using a specific weight, w, of 450 grains per inch cubed. Table I contains appropriate constants for computing fragment velocities using Equation (12).

Plate glass (0.25 inch thick) shatters into pulverized powder which exhibits very little penetrating power. Spray patterns are elliptical and well defined. Total horizontal dispersion is typically about 50 degrees, 25 degrees on either side of γ; typical vertical dispersion is ± 20 degrees. Laminated safety glass (0.193 inch thick) yields larger fragments as well as powder. Fragment yield is limited essentially to the material directly involved in the ballistic impact. Spray angles at 0 degrees obliquity, 90 degrees yaw, were about ± 5 degrees in the horizontal and ± 24 degrees in the vertical direction. At 45 degrees obliquity (CCW) and 45 degrees yaw (CW), horizontal dispersion extends from α_X = -55 degrees to α_X = 10 degrees, and vertical dispersion is again about ± 24 degrees. Plexiglas, type 55, yields many "flake-like" secondary fragments which quickly lose velocity in air and which have very little penetrating power. Dispersion patterns are similar to those of glass. Reference to Figures 17 and 18 reveals that the dispersion patterns are similar to those of aluminum cast materials, as would be expected. Fragment velocities associated with these materials tend to exceed those of aluminum fragments; Equation (7) pertains and has larger values for these materials. Maximum velocities are associated with γ as predicted by Equation (13) or (28).

Wire bundles, approximately 1 inch in diameter and containing approximately 25 individually wrapped stranded wires, broke the yawing projectiles and generated hundreds of wire splinters. Some of these splinters hit end-on and penetrated over an inch of Celotex. Total spray angles exceeded 50 degrees. Steel tubing, 1 inch in diameter (0.049-inch wall) impacted at impact obliquities of -45 degrees by projectiles yawed at 45 and 90 degrees produced large fragments (25 to 45 grains) which had directions in the range of $\beta_x = 0$ to $\beta_x = -40$ degrees.

In a series of tests against flight instruments and navigational aids, using the X-ray system for determination of fragment spray patterns, it became evident that results of projectile impact into such components are completely unpredictable.

IV. DESIGN CONCEPTS FOR SUPPRESSANT SYSTEMS

4.1 SUPPRESSANT DESIGN CRITERIA

The following criteria are fundamental for design considerations:

1. Suppressant will not stop the bullet and, therefore, should perturb the bullet's flight no more than absolutely necessary.

2. Suppressant must not, itself, become a source of potentially damaging secondary fragments.

3. Suppressant must absorb secondary fragment energy efficiently; energy absorption to weight ratios must be as high as possible.

4. Design concepts must be convertible to practical designs.

4.2 FUNDAMENTAL DESIGN CONSIDERATIONS

To stop a secondary fragment, a thickness of material must absorb the total momentum of the fragment. This momentum transfer is accomplished by shear waves which move outward radially from the point of impact. Ballistic impact involving a blunt fragment produces maximum shearing stresses in the target material at the fragment periphery. If the shearing strength is not exceeded at the periphery, the shear waves will proceed laterally into the material following a radial tensile wave created by the rotational component of the shear. The resulting combination of strains may produce a tensile failure. Critical velocities are associated with the creation of both (1) shear failure at the fragment periphery and (2) tensile failure near the fragment periphery. If the fragment perforation velocity exceeds one of these critical values, perforation will occur and the fragment will retain a major portion of its initial kinetic energy.

$$V_{\tau c} = \frac{\tau_c}{\rho U_{\tau c}} \quad \text{(Shear failure)} \tag{29}$$

$$V_{\sigma c} = \sqrt{\frac{\sigma_c U_{\sigma c}}{\rho(U_{\sigma c} + U_{\tau c})} - \frac{U_{\sigma c}^2 U_{\tau c}^2}{(U_{\sigma c} + U_{\tau c})^2}} \quad \text{(Tensile failure)} \quad (30)$$

where $V_{\tau c}$ is maximum (critical) velocity which can be sustained in direction of projectile motion - shear (in./sec)

$V_{\sigma c}$ is maximum (critical) velocity which can be sustained in direction of projectile motion - tensile (in./sec)

τ_c is critical shear stress (psi)

σ_c is critical tensile stress (psi)

ρ is mass density $\frac{(\text{lb sec}^2)}{\text{in.}^4}$

$U_{\tau c}$ wave velocity at critical shear stress (or strain) (in./sec)

$U_{\sigma c}$ wave velocity at critical tensile stress (or strain) (in./sec)

The lowest critical velocity determines the limit of the material to sustain ballistic impact without failure (the critical velocity is not the ballistic limit velocity but is influential in determining its value). For two-dimensional perforation geometries (fragment impacting a strand of yarn; a long rod impacting a sheet of material parallel to its axis) these equations represent singular values of critical velocity. For three-dimensional perforation geometries (a fragment impacting a sheet of material), the equations represent only limiting values of critical velocity (perforation will always occur when fragment perforation velocities exceed limiting values). Lower velocities will cause failure, these lower critical values being functions of total displacement and fragment dimensions. The equations do provide the means for selecting materials possessing high critical velocities but do not predict perforation velocities.

Solution for τ_c, σ_c, $U_{\tau c}$, $U_{\sigma c}$, requires development of true-stress (σ) true-strain (ϵ) relationships, which will usually take the following form:[4]

$$\epsilon = \frac{\sigma}{E} + \left(\frac{\sigma}{K}\right)^{1/n} \tag{31}$$

$$\text{or} \quad \epsilon = K_1 + K_2 \ln \sigma \tag{32}$$

where true-stress at failure is:

$$\sigma_c = \frac{(\sigma_{eng})c}{1 - R_A}$$

and true-strain at failure is:

$$\epsilon_c = \ln \frac{A_0}{A}$$

Such relationships are not generally available for the variety of materials that might be considered for suppressants. Further, dynamic stress-strain relationships appropriate to the ballistic impact problem are usually nonexistent. Those that do exist are questionable because the state of the art does not yet include an accurate technique for obtaining dynamic true-stress true-strain values.

Table IV presents some critical velocity values calculated using Equations (29) and (30) and data available in the literature.[4,5] While the values themselves should not be taken seriously, they establish certain guidelines. The metals are not truly candidates for several reasons. In order to reduce secondary fragment velocities to the critical values listed, metal plates would have to be of the same order of thickness as the fragments. Consequently, they would act as fragment generators, simply transferring the problem from one place to another. The dynamic values listed for the felt fibers and polyethylene fibers indicate that they will be perforated easily by fragments having velocities above 2000 feet per second. The values given are limiting values; actual critical velocities for the fragment impact geometry will be much less, perhaps about 1000 feet per second. A single thickness of felt would stop the fragment only after momentum transfer to the material directly ahead of the fragment had reduced its velocity to the critical value. Consequently, felt pads used independently would have to be quite thick. However, the energy absorption capabilities of felt materials on a weight per unit thickness basis greatly exceed those of metals, and felt materials should not be discarded as candidates for suppressant systems.

TABLE IV

APPROXIMATE CRITICAL VELOCITIES FOR SEVERAL MATERIALS
(Based on Best Stress-Strain Data Found)

Material	Stress-Strain Data Obtained at This Strain Rate (in./in./sec)	Limiting Critical Velocities	
		Shear (ft/sec)	Tension (ft/sec)
Felt Fibers (Nylon, Isostatic Polypropylene)	0.0002	1900	2100
	30,000	1200	--
Polyethylene Fibers	30,000	1900	2900
2024 Aluminum (Annealed)	Static	850	850
Mild Steel	Static	1000	850
Glass reinforced epoxy	0.0002	490	950

TABLE V

LIST OF MATERIALS EVALUATED AS SUPPRESSANTS

A. Opaque Materials

1. Synthetic Felts (Nylon, Polypropylene, Dacron and Orlon; areal densities from 19 to 53 ounces per square yard)
2. Code 710 Check Strap Material, five-ply rubber-bonded cloth woven nylon on external surfaces, three-ply woven cotton core
3. "Texhide", five-ply rubber-bonded cloth, center ply woven nylon, two-ply woven cotton outside
4. Celotex, 1/2 inch thickness
5. Glass reinforced epoxy
6. Polyethylene, 0.060 inch thickness
7. Cloth reinforced rubber, 0.093 inch thickness
8. Code 720 rubber-bonded woven nylon (two-, three-, and four-ply samples).

B. Transparent Materials

1. Estane
2. Lexan, 0.060 inch thickness
3. Polyvinyl, 0.040 inch thickness
4. Tenite Butyrate, 0.060 inch thickness
5. Surlyn "A", 0.030 inch and 0.060 inch thicknesses

The foregoing leads to the following observations regarding fundamental design considerations:

1. A single material used as a suppressant must act as an armor to secondary fragments while affecting the projectile as little as possible. It must have sufficient areal density to reduce the perforation velocity of the fragment below a critical value.

2. Materials such as felts will find application in suppressant systems only in combination with other materials which precondition fragments so that the energy absorbing material can absorb the remaining momentum of the fragments.

3. Reduction in fragment velocity, increase in fragment presented area, and smoothing of the fragments' contours represent means for reducing the perforating capability of secondary fragments (increasing critical velocity).

Three suppressant design concepts were investigated experimentally. The first concept involved comparisons of single materials (including bonded laminates) in their capability to defeat typical secondary fragments. The second and third concepts incorporate means for modifying fragment velocity, increasing fragment presented area, and smoothing fragment contours, prior to absorption of fragment momentum by a backup material. For example, Celotex tends to ball up in front of the fragment, performing all the functions identified in the third observation listed above. Backed up by a nylon laminate, or a felt, it succeeds in defeating typical fragments. To study dual function suppressants under controlled conditions, metallic and nonmetallic platelet mosaics were backed up by absorber materials. The controlled-size platelet geometry was far less successful than other dual function geometries. However, initial experiments were limited in scope, and a more thorough study might reveal means to optimize platelet geometries.

4.3 CONTROLLED PLATELET CONCEPT

Lightweight felt materials and other similar materials can absorb a great deal of energy provided that fragment velocities are reduced well below the critical velocities associated with these materials. Reduction of secondary fragment velocity can be accomplished by using small

platelets in front of the felt, sized so as not to be perforated by the secondary fragment while accepting momentum from the fragment. The remaining normal velocity of a fragment-platelet combination is given by:

$$(V_{rs})_n = \frac{W_f}{W_f + W_s} V_0 \cos \theta_s \tag{33}$$

provided that the platelet is not perforated. Perforation velocity of the platelet can be predicted using the equation:

$$V_{xl} = \frac{(V_{xn})_b}{\cos \theta_s} \sqrt{\frac{1 + W_f/W_s}{1 - \frac{W_{so}/\cos \theta_s}{W_s}}} \tag{34}$$

where $(V_{rs})_n$ is remaining velocity of platelet (ft/sec)

V_0 is impact velocity (ft/sec)

V_{xl} is platelet perforation velocity (ft/sec)

$(V_{xn})_b$ is minimum perforation velocity for a large plate of the platelet material having the same thickness as the platelet (ft/sec)

θ_s is impact obliquity angle of the secondary fragment at the suppressant

W_f is secondary fragment weight (grains)

W_s is platelet weight (grains)

W_{so} is the weight of a platelet plug having the same presented area as the secondary fragment (grains)

The weight of the platelet can be written as:

$$W_s = (bw_s) A_s \tag{35}$$

where b is thickness (in.)

w_s is specific weight $\left(\frac{\text{grains}}{\text{in.}^3}\right)$

(bw_s) is areal density $\left(\frac{\text{grains}}{\text{in.}^2}\right)$

A_s is platelet area (sq in.)

Since the thickness, (b), establishes the value for $(V_{xn})_b$ for any platelet material, and since the impact velocity, V_0, is the minimum value that V_{xl} can have, Equation (34) can be solved for the minimum area, A_s, that a platelet can have and not be perforated. A value of areal density, bw, is assumed, establishing $(V_{xn})_b$; V_{xl} is set equal to V_0; and Equation (35) is substituted in Equation (34). Once W_s has been determined for given values of areal density and platelet area, Equation (33) can be solved to determine the remaining velocity of the nonperforated platelet.

A typical aluminum secondary fragment having a weight W_f of 9.6 grains, a presented area of 0.0984 square inch, an impact velocity of 2430 feet per second, and an obliquity, θ_s, of 25 degrees was used to develop the curves for five platelet materials shown as Figure 19. The upper curves relate maximum platelet area to areal density. The vertical lines on this plot represent the areal density of large plates of the same material which would be required to stop the fragment. The lower curves show the resulting residual velocity. To cite an example, suppose that the platelet fragment remaining velocity must be reduced to 750 feet per second to be stopped by a felt material having an areal density of 40 ounces per square yard (14 grains per square inch). If the platelet is made of aluminum, an areal density of 80 grains per square inch is the minimum which the platelet can have (lower curves). On the upper curves, this areal density corresponds to a platelet area of 0.18 square inch, a platelet of 0.42 inch on a side. The total areal density of the felt-aluminum suppressant system is 94 grains per square inch; an aluminum plate of almost twice this areal density would be required to stop the fragment. Ballistic limit values used in the computations are obviously quite conservative, and it is probable that suppressant systems having areal densities of about 50 grains per square inch (150 ounces per square yard) can be developed. Metal platelets would probably not be used in actual designs, since they

appear to be less efficient and would be driven through the felt by the projectile and would thereby represent a new threat.

The typical fragment described in the previous paragraph is the largest fragment predicted for the $\theta = 45$ degrees (CCW), $\phi = 90$ degrees (CW) impact condition involving an aluminum rolled plate, 0.063 inch thick (refer to Figures 16 and 18) perforated by a caliber .30 projectile having an initial velocity of 2500 feet per second. This geometry represents a severe test for suppressants and was used as a standard for most of the suppressant tests. Test No. 202 is typical of the suppressant tests involving platelets. This test is diagrammed on Figure 20. The yawing ball projectile retained a velocity of 1990 feet per second after passing through the 0.063 inch aluminum plate. Secondary fragments in the direction of the suppressant had velocities characterized by the fragment which missed the suppressant and had a velocity of 1925 feet per second. Thirty Texhide No. 2 platelets, each weighing 14 grains (0.6 × 0.6 inch squares), were mounted on 1/8-inch nylon felt. Two major secondary fragments perforated the platelets as shown, retaining velocities of 660 and 620 feet per second. Failure of the suppressant system was attributed to failure of the platelet material, which was cut by the sharp fragments. The platelets were contained by the felt.

V. EXPERIMENTAL EVALUATION OF SUPPRESSANT SYSTEMS

In foregoing discussions, it was established that ballistic impacts into plates under conditions specified for this program produced predictable results and that results of low-velocity tests could be predicted with reasonable accuracy. This allowed the omission of a great number of low-velocity tests in favor of tests to evaluate spall suppressants. The impact conditions which created the greatest hazard to personnel were used in evaluation of spall suppressants. For opaque materials, these conditions involved 0.063-inch-thick aluminum plate or 0.250-inch-thick aluminum castings at 45 degrees obliquity, impacted by either ball or AP projectiles at 2500 feet per second and 90 degrees yaw. Results of tests in which 0.020-inch-thick aluminum witness sheets were placed behind the targets without suppressants are illustrated in Figures 22 and 23. Figure 22 illustrates the hazard created by impact of aluminum casting under the above conditions; (Figure 23 illustrates the typical hazard created by impact of aluminum sheets under these conditions.) Figures 24 through 28, to be referred to in following discussion, are photographs of 0.020-inch-thick witness sheets used in evaluation of suppressants and may be compared directly to either Figure 22 or 23. Target material and/or a mockup of the suppressant system is shown in the lower left hand corner of the above photographs.

Preliminary tests with various candidate spall suppressants were conducted early in the program to provide an experimental basis for development of a satisfactory suppressant system. In this preliminary program, one fact became immediately obvious: a suppressant of reasonable thickness placed in contact with or bonded to the back surface of a target specimen has negligible effect on fragments driven from the impacted area. The reason for results of this nature may be more readily understood by study of the sequence of four high-speed photographic exposures in Figure 9. In Frame 1, the ball projectile has just broken through the aluminum casting and the fragments are still in close proximity to the projectile. If the projectile and fragment cluster encounter a suppressant at this time, most of the fragments will continue to be propelled by the projectile and thus cannot be stopped by the suppressant (see Figures 24 and 25). In Frame 2, the projectile is about 1-1/2 inches past the point of impact and most of the fragments have now become separated from the projectile. If the projectile and fragment cluster encounter a suppressant under these conditions, the projectile will punch a hole in the suppressant; but each

individual fragment which is not on the line of flight of the projectile can pass through the suppressant only if its own kinetic energy is high enough to overcome the resistance offered by the suppressant (see Figures 26 and 27). The candidate suppressants which were evaluated in the early stages of the program included synthetic felts, cloth-reinforced rubber sheeting, and two types of five-ply rubber bonded material. These preliminary tests served to bracket the problem. The two five-ply materials were most effective in stopping the fragments generated under the impact conditions which had been shown to present the greatest hazard.

In continuing evaluation of candidate suppressant materials, those listed in Table V were tested singly and in combination with each other. The test procedure was the same as described for tests without suppressants except that the suppressant was mounted behind the plate as shown in Figure 21. Thus, characteristics of debris generated as the projectile passed through the suppressant were also determined. Several of the materials tested proved to be capable of stopping all secondary fragments from the aluminum plate but were classed as unsatisfactory because the projectile punched out a hazardous fragment from the suppressant itself.

The synthetic felts were generally ineffective in stopping secondary fragments when used singly (see Figure 28), but showed promise when used in conjunction with platelets or Celotex. The lightest weight material which showed satisfactory characteristics in early evaluation was Texhide (areal density, 115 ounces per square yard). It was decided that the areal density could be reduced if laminations of nylon only were used in the suppressant material.* Several samples of rubber-bonded two-, three-, and four-ply woven nylon laminated and press-cured were prepared for evaluation on this program.

Of the various materials and material combinations evaluated on this program, a four-ply nylon proved to be the lightest material capable of stopping the most hazardous fragments generated under this program. The areal density of this material is 77 ounces per square yard. The fibrous particles punched out of this suppressant by the projectile were fluffy and nonhazardous. The best results were obtained when the spacing between the target plate and the suppressant was no less than 1-1/2 inches. The effectiveness of this suppressant is illustrated in Figures 26 and 27.

* This conclusion was in line with suggestion of operating units in Viet Nam (see Reference 6).

The hazard due to secondary fragments from ballistic impact of transparent materials tested was less severe than that from structural materials (Figures 29 and 30); i.e., these fragments were generally smaller and lighter and therefore has a lower potential for incapacitation of personnel, especially if the facial area is protected. Obviously, any suppressant proposed to be used in conjunction with transparent materials should also have good optical qualities. Several clear plastic materials were evaluated as suppressants against fragments generated by projectiles at 2500 feet per second and 90 degrees yaw impacting laminated glass and acrylic plastic at 45 degrees obliquity. All of these suppressant materials were found to produce secondary fragments themselves as the projectile passed through.

The transparent suppressant material which gave the best overall performance was 0.060-inch Surlyn A. Required spacing between target plate and Surlyn A was 2 inches. Under these conditions, most of the fragments were stopped as illustrated in Figure 31. However, in addition to the fact that the hazard was not completely eliminated by use of Surlyn as a suppressant, other problems could be created when using this material:

1. Debris driven from laminated glass and acrylic plastic contained a large amount of very small dustlike particles which appeared to be electrically charged; therefore, they were attracted to and deposited on the surface of the plastic suppressant, reducing light transmission.

2. An area of approximately 10 square inches was rendered opaque by direct impingement of energetic debris particles.

3. Dust could collect between the suppressant and the windshield in normal operation, creating a maintenance problem.

In view of the above facts, it may be considered advisable to provide adequate body protection (i.e., visors, heavy clothing) to the personnel in the cockpit area in order to avoid the complication of a backup for the primary transparent material. Of the primary transparent materials tested, the material which produced the least hazardous fragments due to impact was stretched acrylic plastic (MIL-P-25690A). This material also showed the lowest loss of visibility due to ballistic impact (see Figure 32).

VI. CONCLUSIONS

It has been shown that velocities and distributions of secondary fragments, generated by ballistic impact of aircraft structural materials, can be predicted when the impact conditions are known. A secondary fragment suppressant system has been developed which is capable of stopping the highest energy fragments (or those fragments representing the greatest hazard to personnel) generated by ballistic impact under conditions specified for this program. This system consists of a bonded, four-ply woven nylon sheet, Code 720, placed with a minimum of 1-1/2 inches clearance on the inside of a surface through which bullet penetration may be expected. The areal density of this material is 77 ounces per square yard.

A completely satisfactory suppressant system to be used in conjunction with transparent materials has not been developed. Transparent materials which could be used as suppressants produce fragments themselves and also introduce maintenance problems.

A suppressant system to be placed on the floor of aircraft and which must carry relatively heavy loads was evaluated. This involves placement of 1-1/2-inch-thick foamed rubber between the four-ply nylon and the floor. Such a system was shown to be capable of stopping most fragments, but it was not optimized; i.e., other materials could probably be selected which would have a lower areal density.

VII. RECOMMENDATIONS

It is recommended that the Code 720 material or a material having equivalent resistance to penetration by fragments be adopted for application as described above, where practicable, to aircraft subject to attack from ground-fired weapons.

In lieu of application of a suppressant to transparent aircraft materials, it is recommended that the transparent material be stretched acrylic plastic wherever possible, since this material produces the least hazardous fragments and suffers the least loss of visibility due to impact. Transparent materials should be as thin as practicable (within strength requirements for operating loads) to further reduce the hazard due to fragments. Personnel in close proximity to transparent materials should wear protective clothing and face visors.

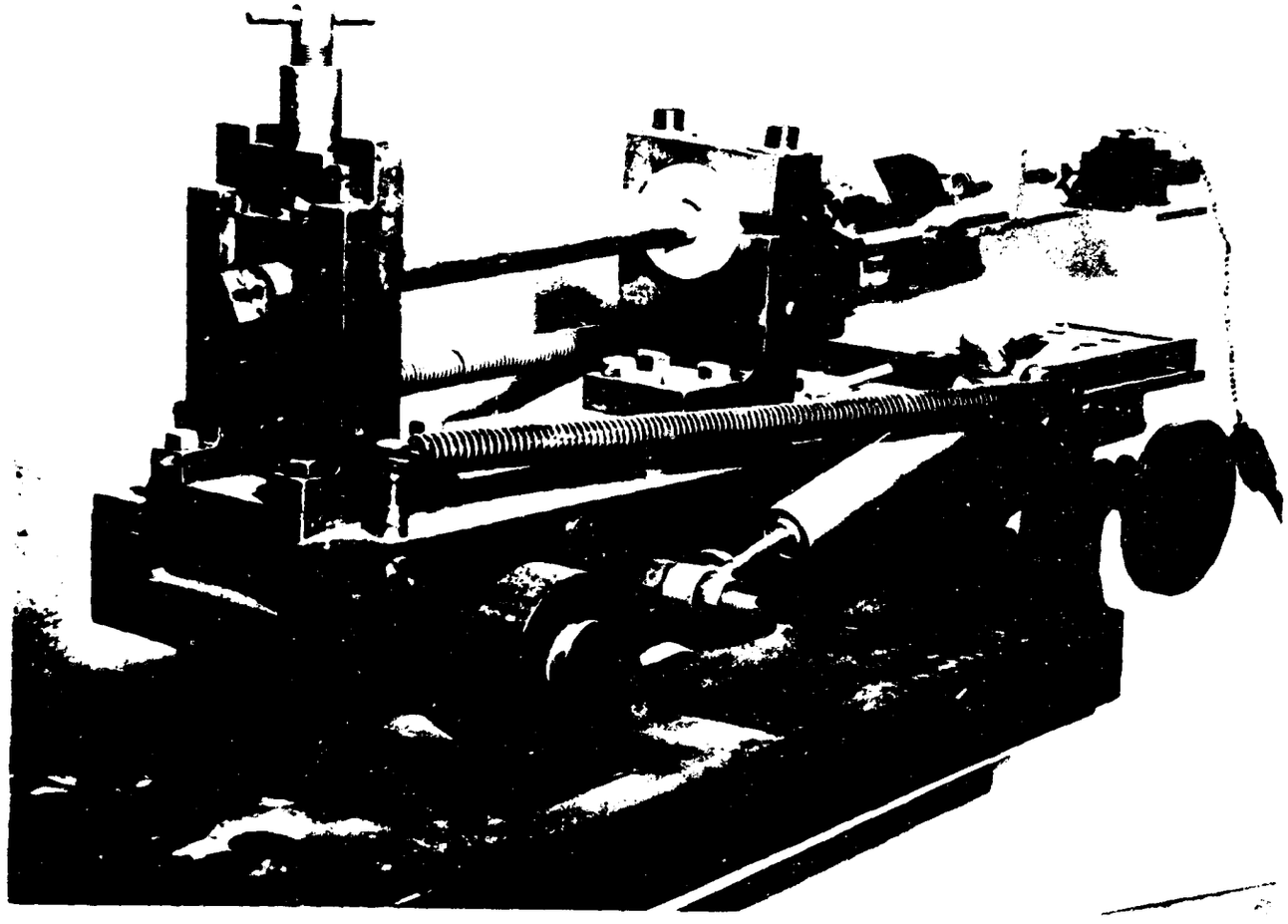

Figure 1. View of Smooth Bore Gun Showing Muzzle Attachment for Producing Projectile Yaw

Figure 2. Close-Up of Yaw-Producing Muzzle Attachment

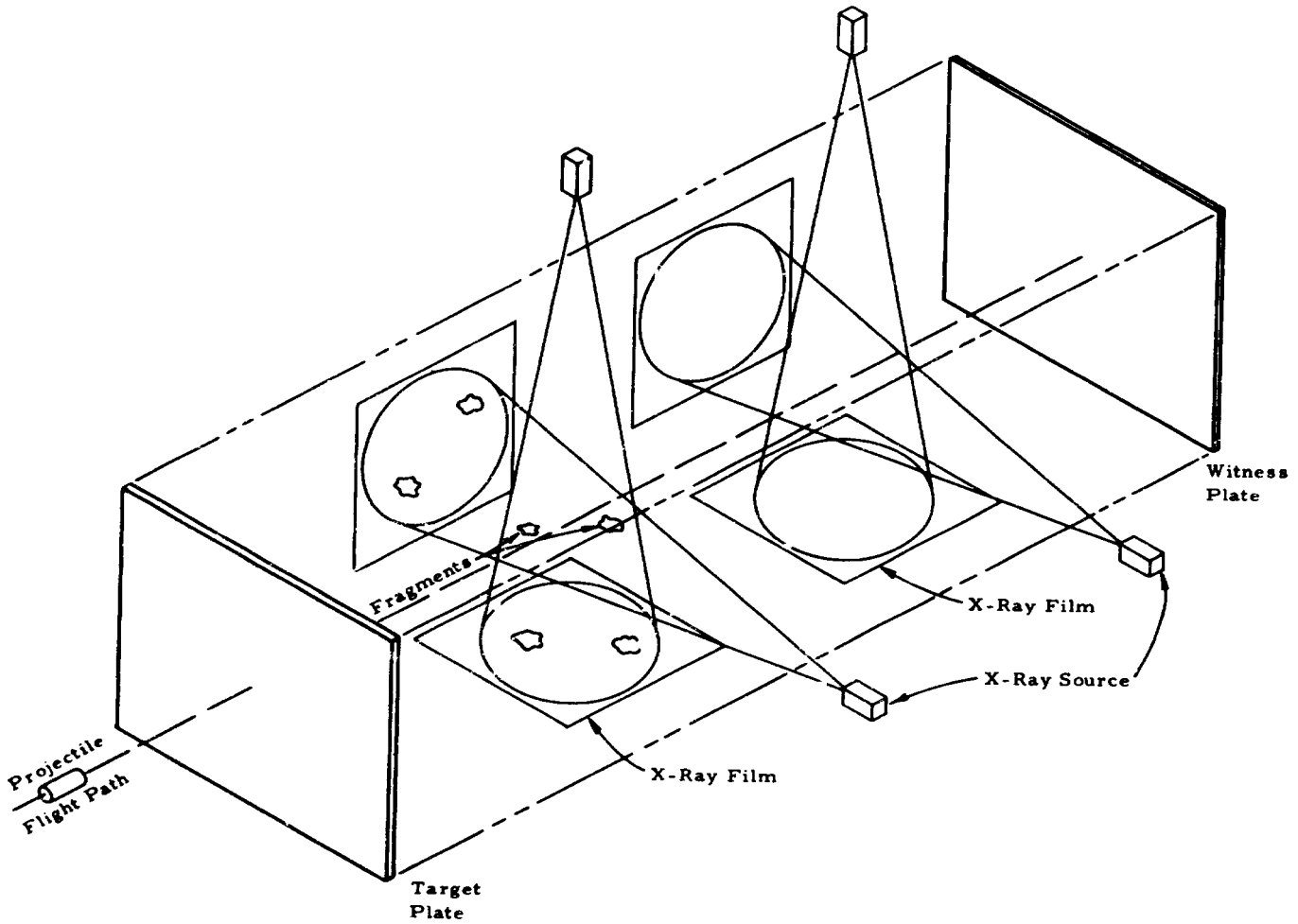

Figure 3. Schematic of Fragment Data Collection System

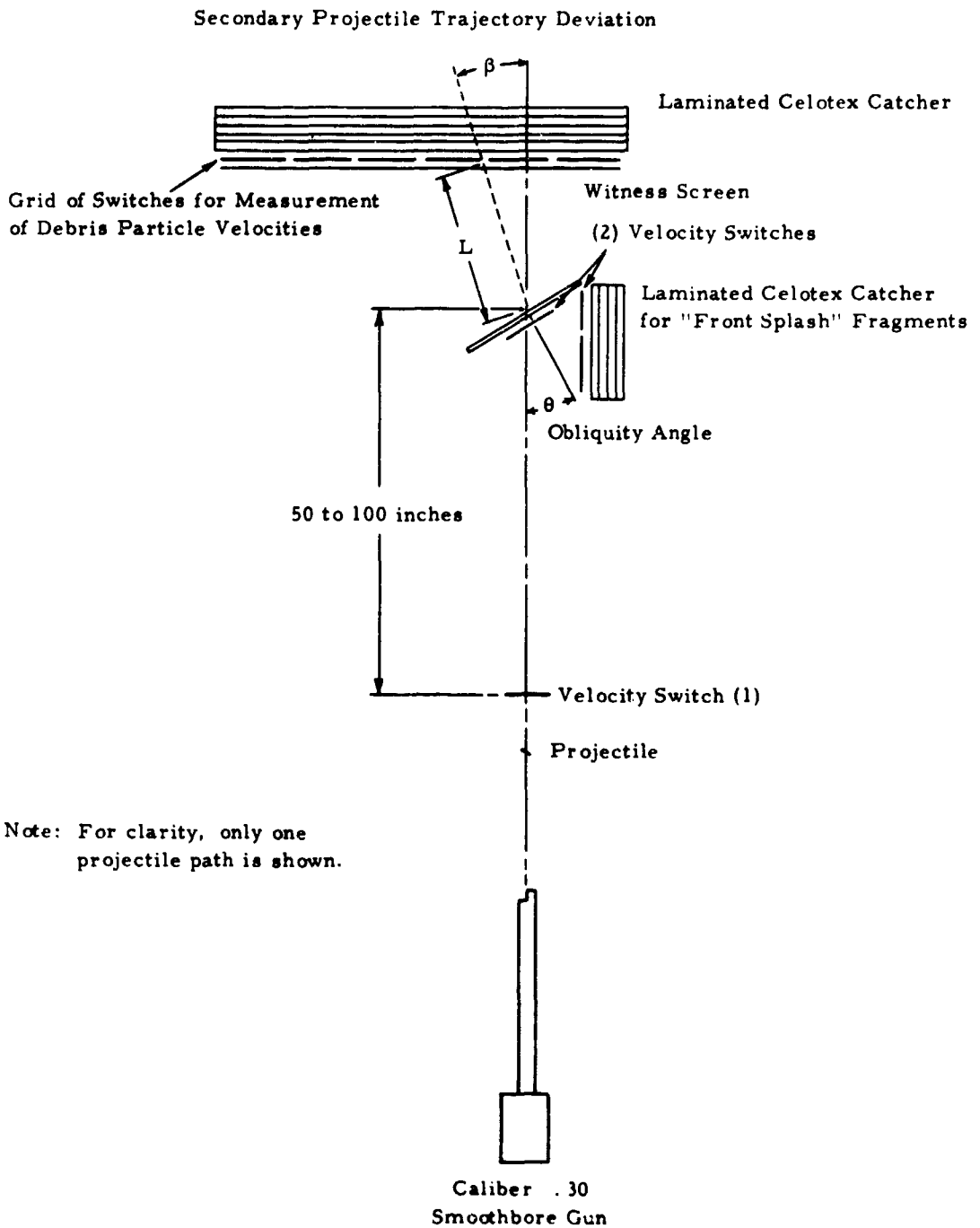

Figure 4. Experimental Arrangement for Determining the Spall and Debris Producing Characteristics of the Several Aircraft Materials and Components

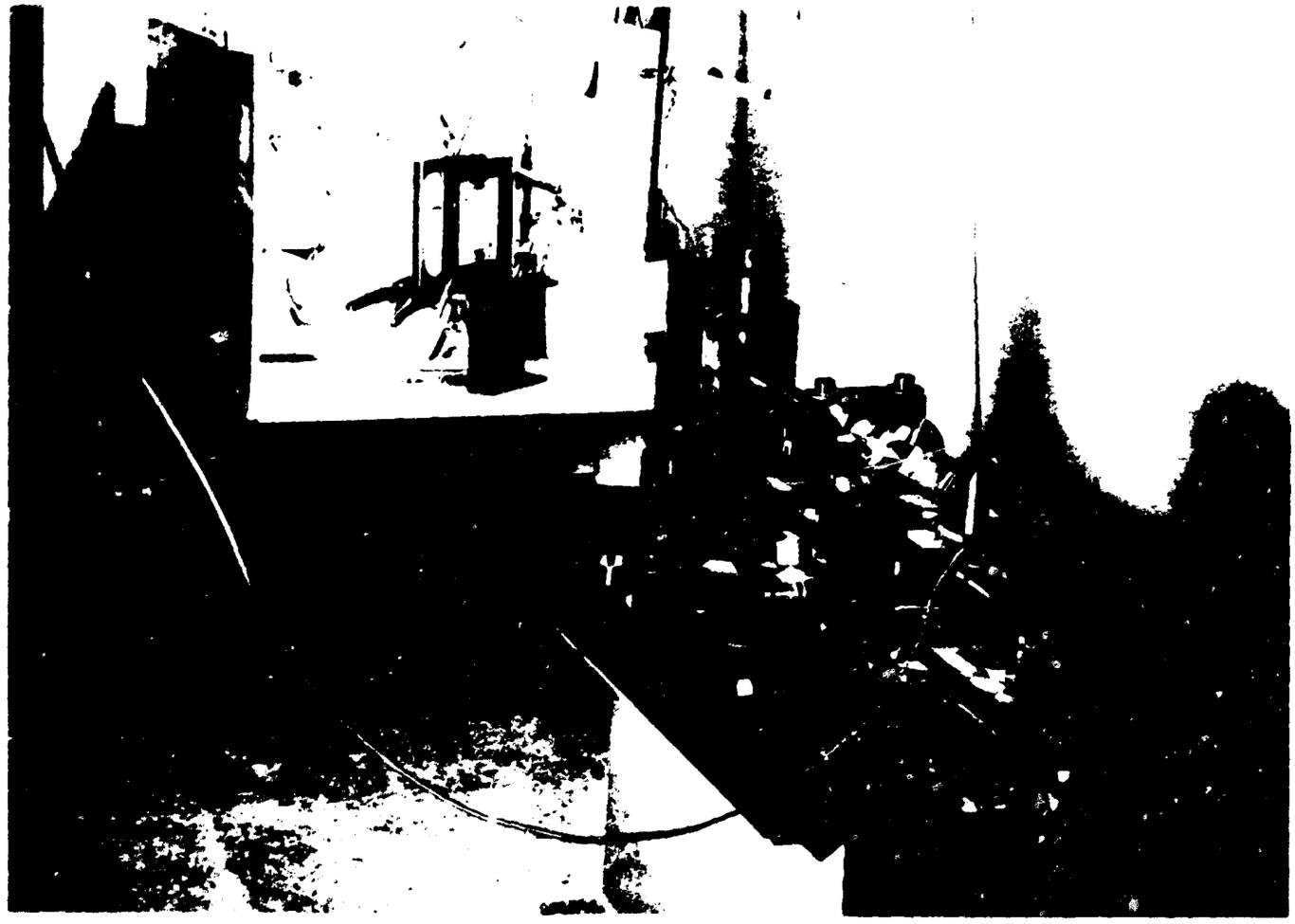

Figure 5. Setup for Ballistic Test of Aircraft Materials

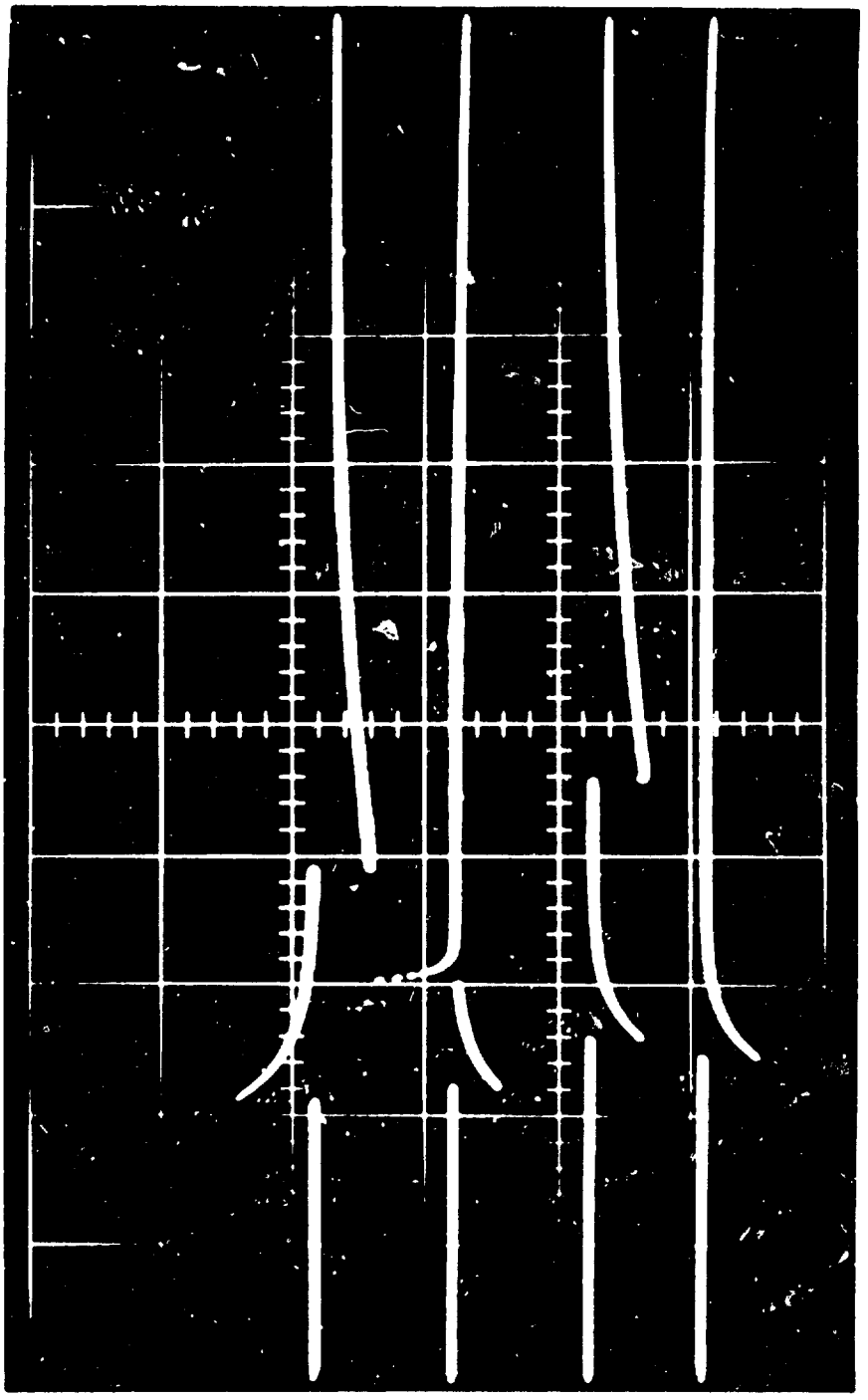

Figure 6. Copy of Polaroid Record from Oscilloscope

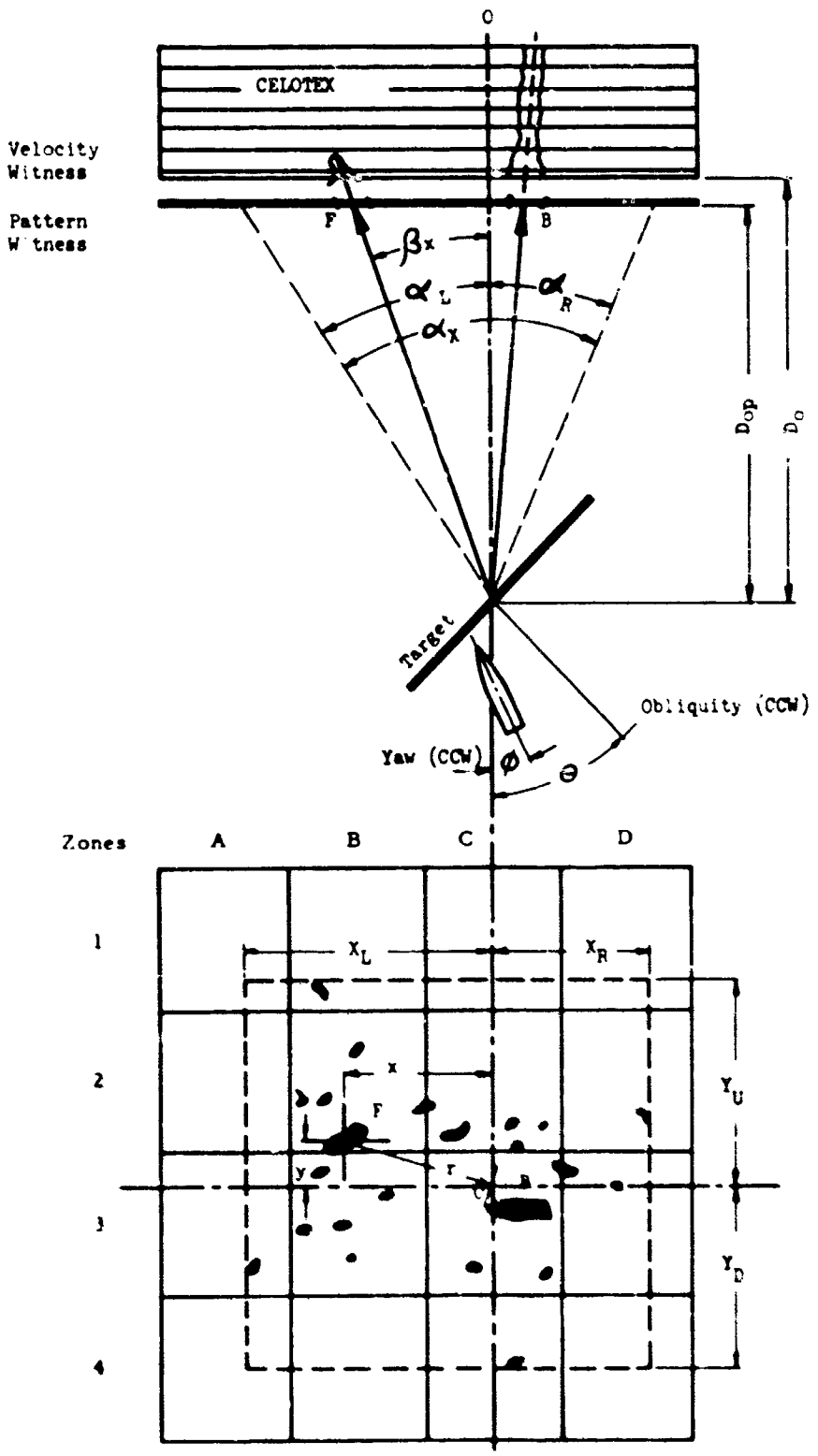

Figure 7. Schematic of Experiment

DRI PROJECT NO. 931
DATA REDUCTION SHEET

TARGET DESCRIPTION:
Material CAST MG
Thickness .262 inch
Other:

Test No. 87 - 31 Aug '66
Projectile & Wt. B-M2(152) (grains)
Impact Velocity 2515 (ft/sec)
Obliquity 45 (degrees CW ___ or CCW X)
Yaw 90 (degrees CW X or CCW ___)
Normal Distance to Velocity Witness D_o 11.75 (inches)
Normal Distance to Pattern Witness D_{op} 11 (inches)

PROJECTILE TERMINAL BALLISTICS:
Residual Velocity (if measured) ___ (ft/sec)
Breakup: Core ___ (yes or no)
Jacket Yes (yes or no)

	Trajectory Intercept								
ZONE:	E4	D4	C4	B4	D3	C3	B3	B2	C5
APPROX. NO. FRAGS.		10	20	5	5	15	5		
MAJOR FRAGMENTS:*	B								
Res. Vel. V_{rf} (ft/sec)	V_{rfn} = 1820	1820	2060	1900	1445	1620	1480	1375	
Weight W_f (grains)			2.6						2.4
Length (inches)			0.35						0.4
Width (inches)			0.25						0.25
Thickness (inches)			0.15						0.15
Shape:		from Vel witness							
x left (inches)		1.0	5.2	5.4	4.5	6.0	10.8	10.3	
x right (inches)									
y up (inches)				1.0	2.8	3.8	3.5	8.8	
y down (inches)			0.5						
r-radius (inches)		1.0	5.3	5.6	5.2	7.0	11.0	13.0	
β_x									
β_y									
β		5°	24°	26°	24°	31°	43°	48°	
cos β		.99	.93	.90	.91	.86	.73	.67	
V_{rfn} cos β		1810	1660	1640	1660	1570	1330	1220	
V_{rfn} cos β / V_{rf}		.99	.81	.87	1.15	.97	.90	.89	
Remarks: μ sec	540	550	545	680	750	700	1000	1060	

BEAM SPRAY ANGLES:
X_L 14 X_R 1 Y_U 11 Y_D 7
α_L 50° α_R 5° α_X 55° α_U 43° α_D 31° α_Y 74°

Approx. No. Major Fragments* ___
Est. Total No. Fragments 200
Est. Total Wt. Fragments (grains) ___

REMARKS: (Details of photographic or X-ray coverage, observations, etc.
Test apparently valid in all respects ___ yes ___ no.

Figure 8. Data Reduction Sheet

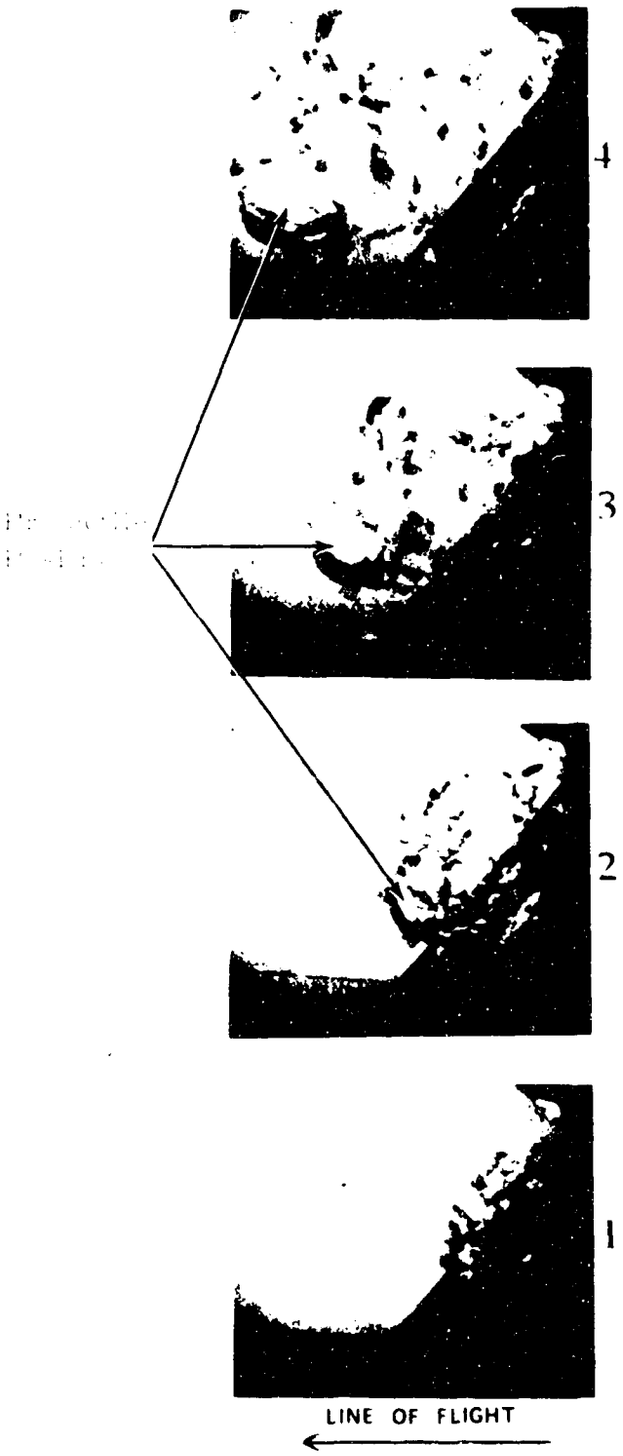

Figure 9. High-Speed Photographs of Secondary Fragments Generated by Ball Projectile During Perforation of Cast Aluminum Plate

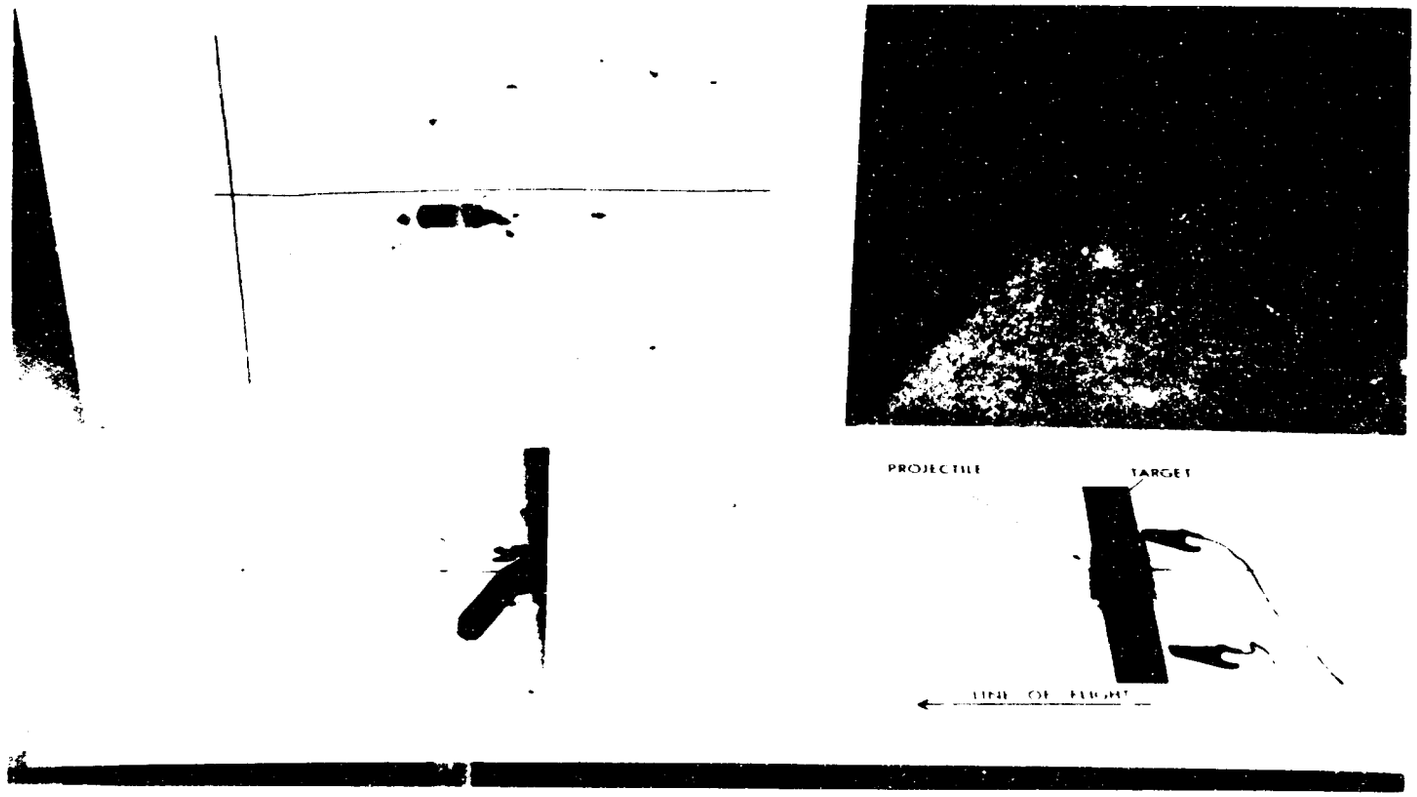

Figure 10. Flash X-Radiographs of Secondary Fragments Generated by Armor-Piercing Projectile During Perforation of Cast Aluminum Plate

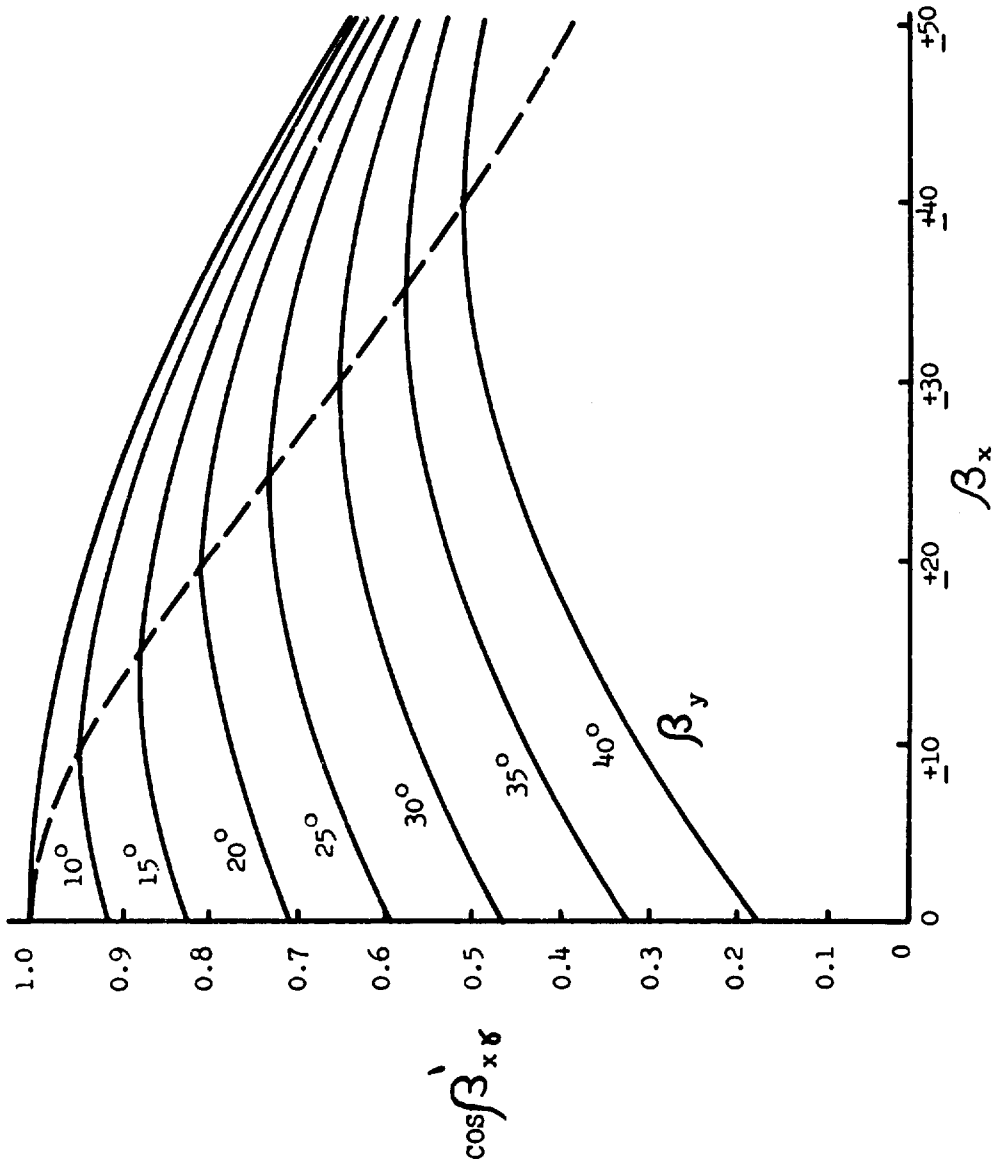

Figure 11. β_x as a Function of Impact Geometry when $\gamma = 0$

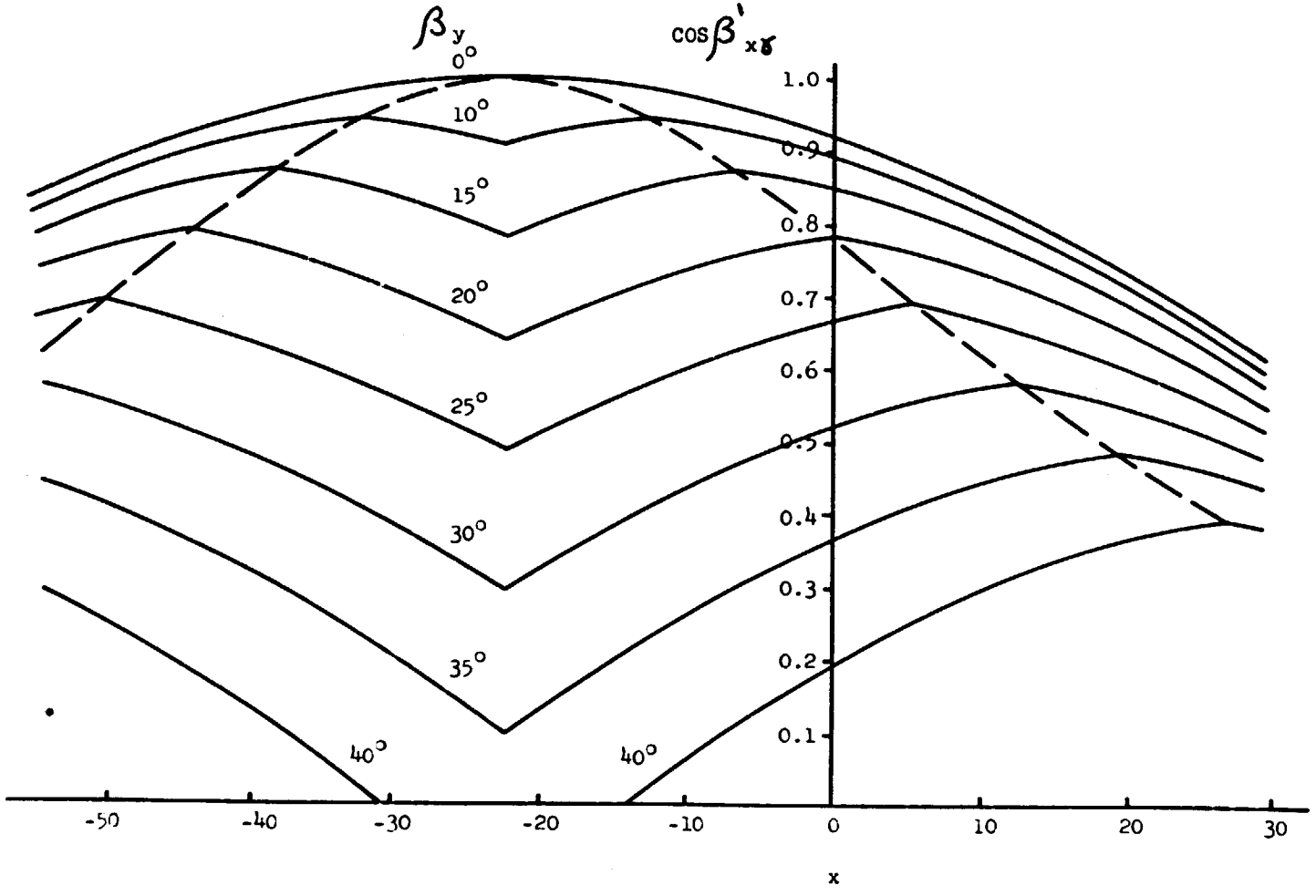

Figure 12. β_x as a Function of Impact Geometry when γ = -22.5 Degrees

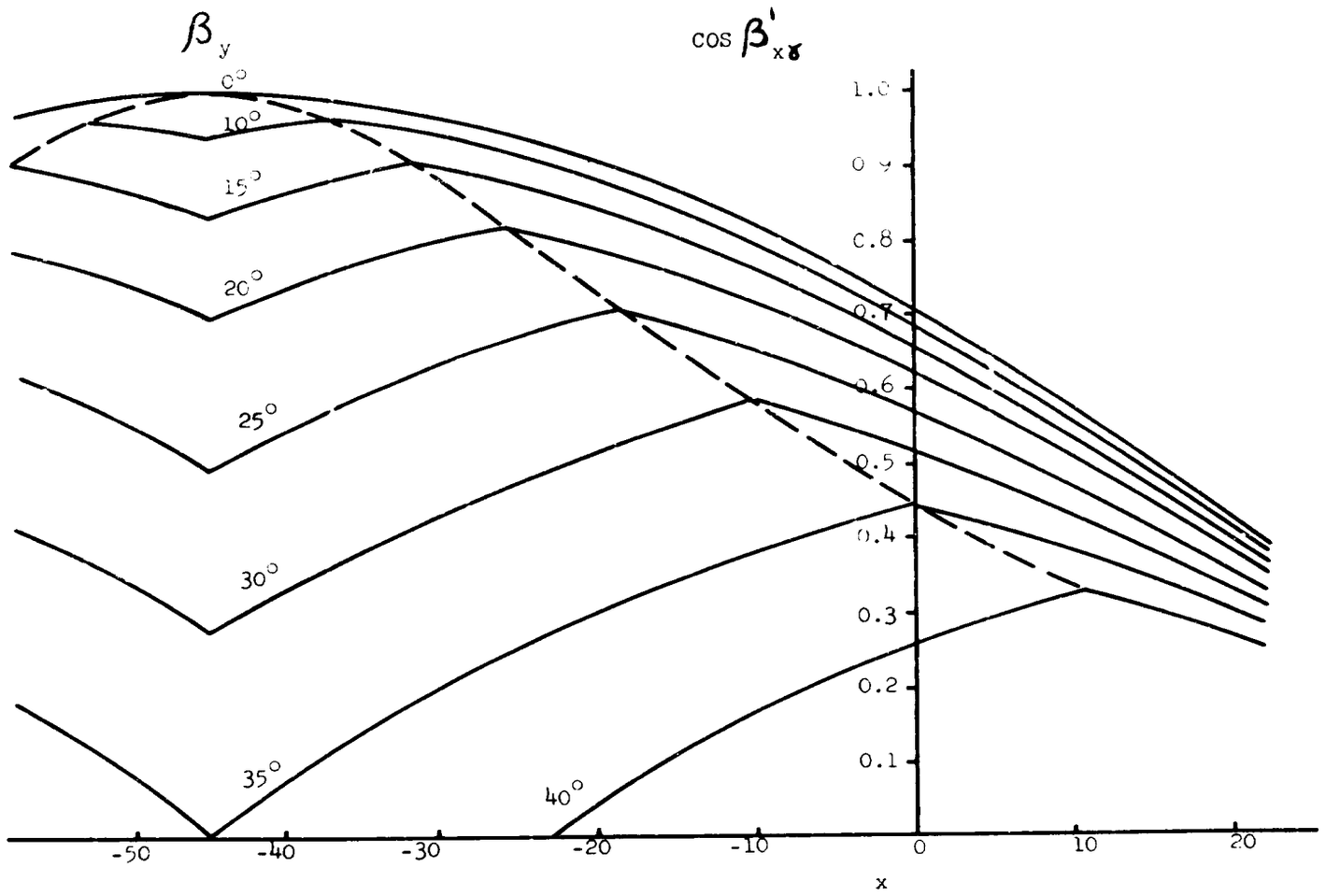

Figure 13. β_x as a Function of Impact Geometry when γ = -45 Degrees

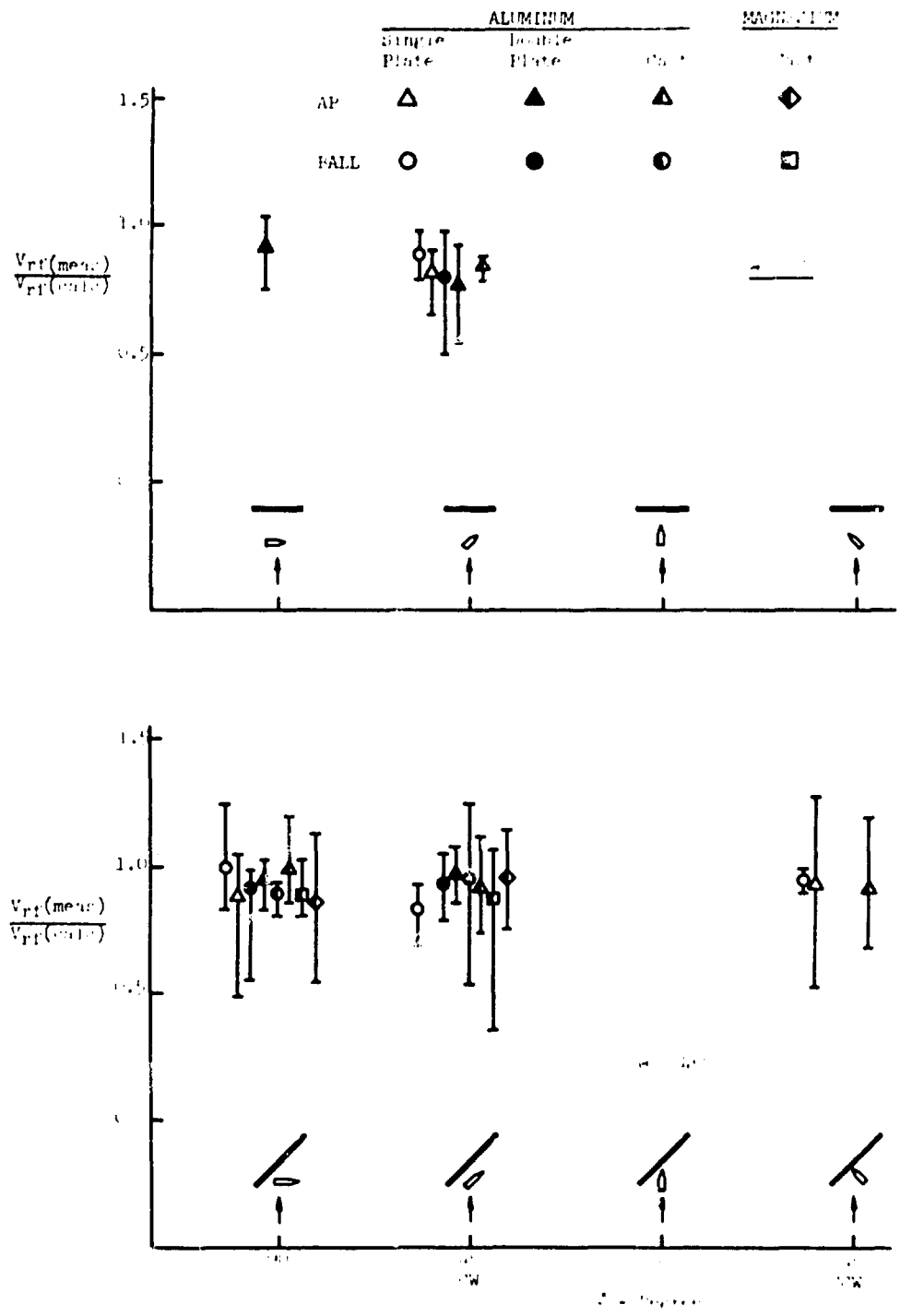

Figure 14. Correlation of Velocity Prediction Equation

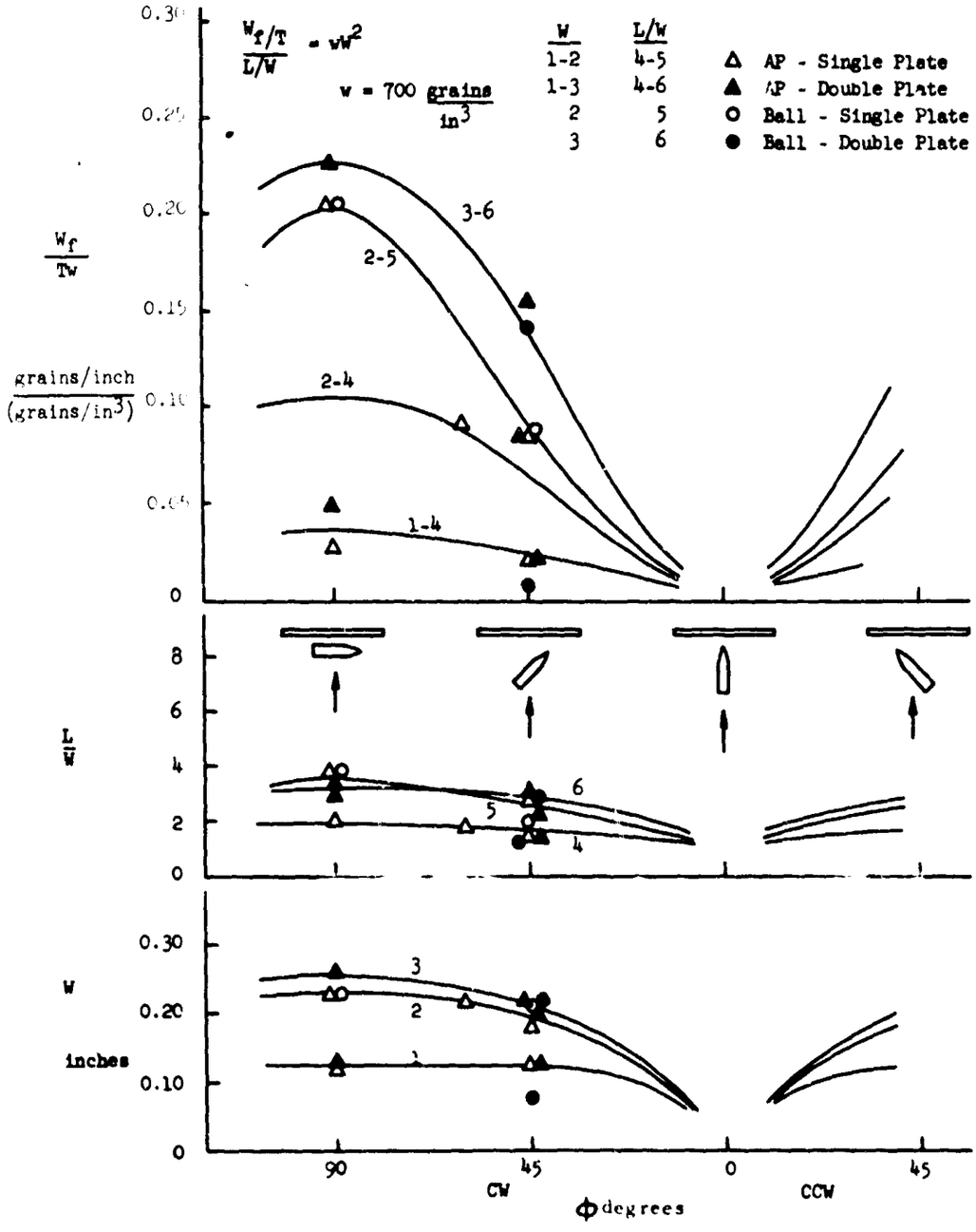

Figure 15. Typical Fragment Weight and Shape Characteristics as a Function of Yaw; Normal Impact Obliquity

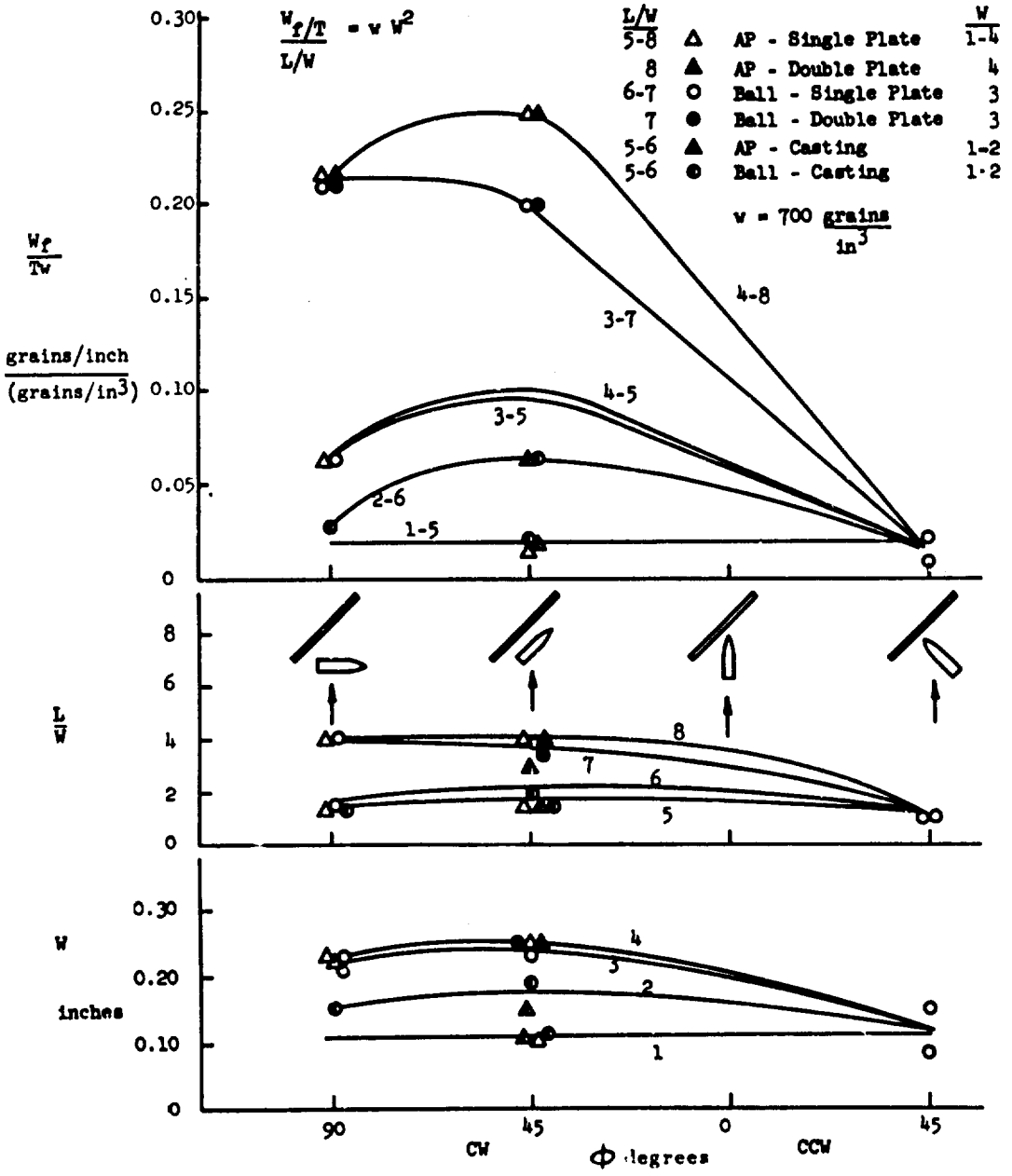

Figure 16. Typical Fragment Weight and Shape Characteristics as a Function of Yaw; Impact Obliquity 45 Degrees

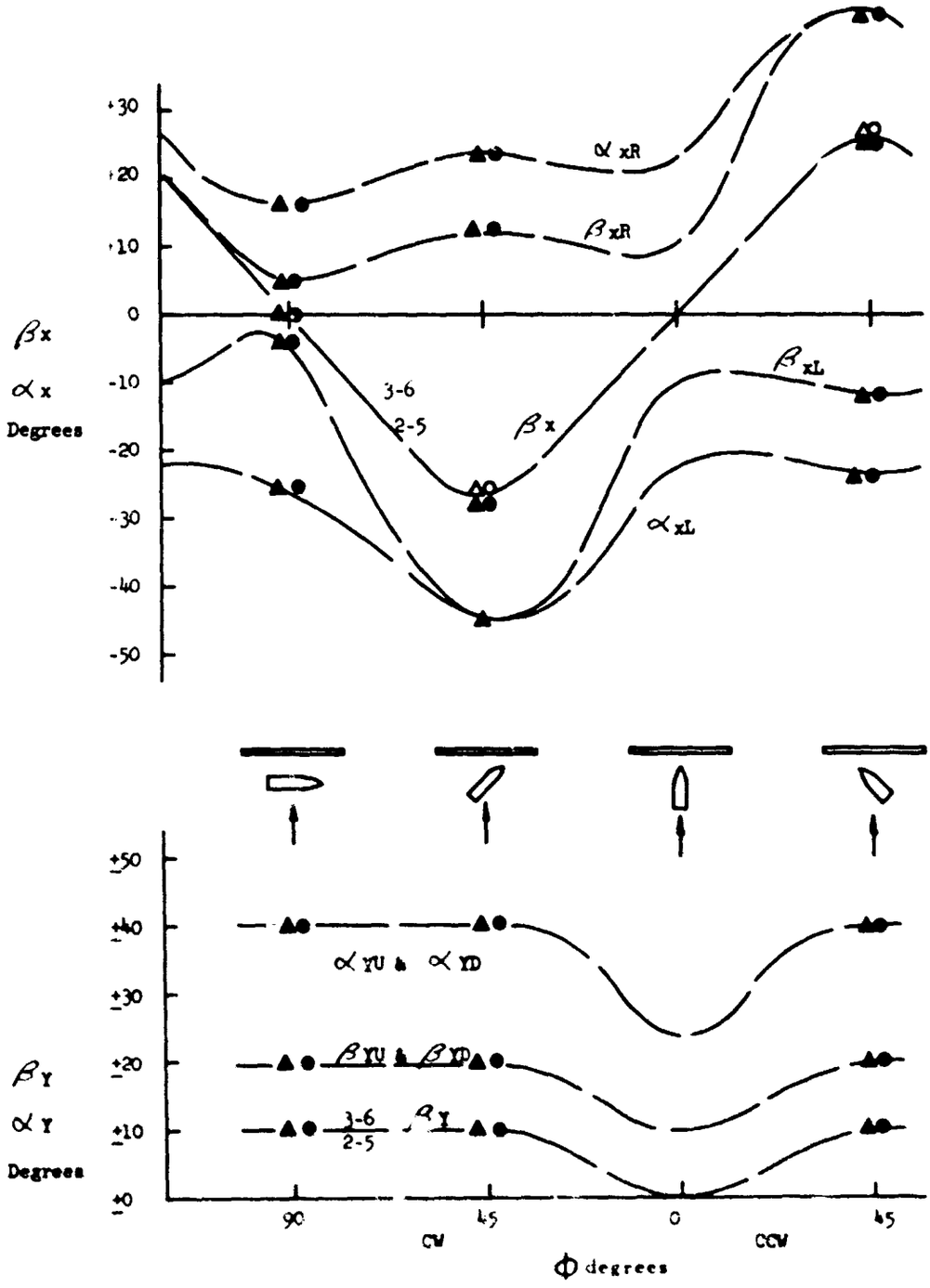

Figure 17. Fragment Direction and Beam-Spray Angles for Major Fragments and Patterns as a Function of Projectile Yaw; Normal Impact Obliquity

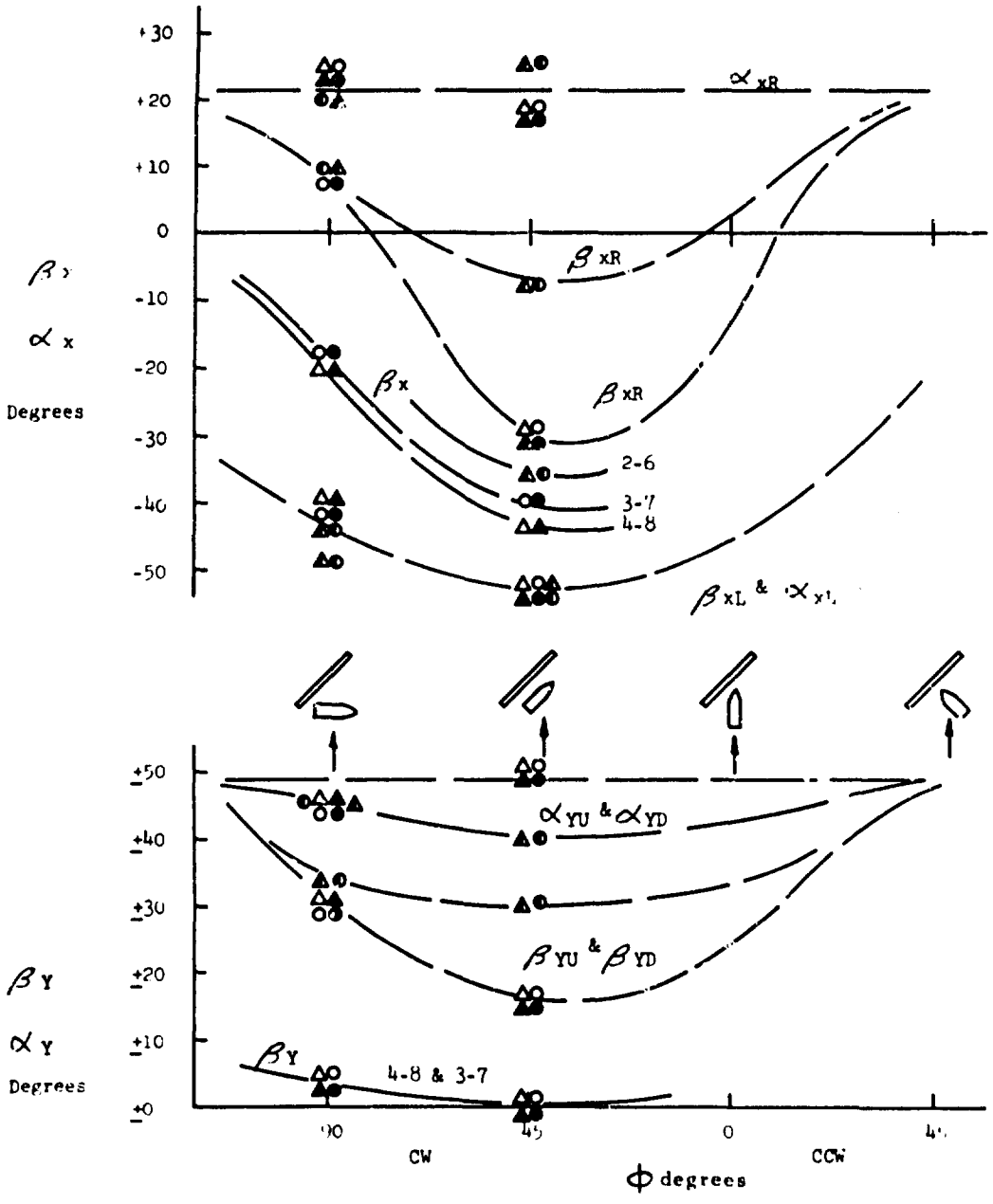

Figure 18. Fragment Direction and Beam-Spray Angles for Major Fragments and Patterns as a Function of Projectile Yaw; Impact Obliquity 45 Degrees

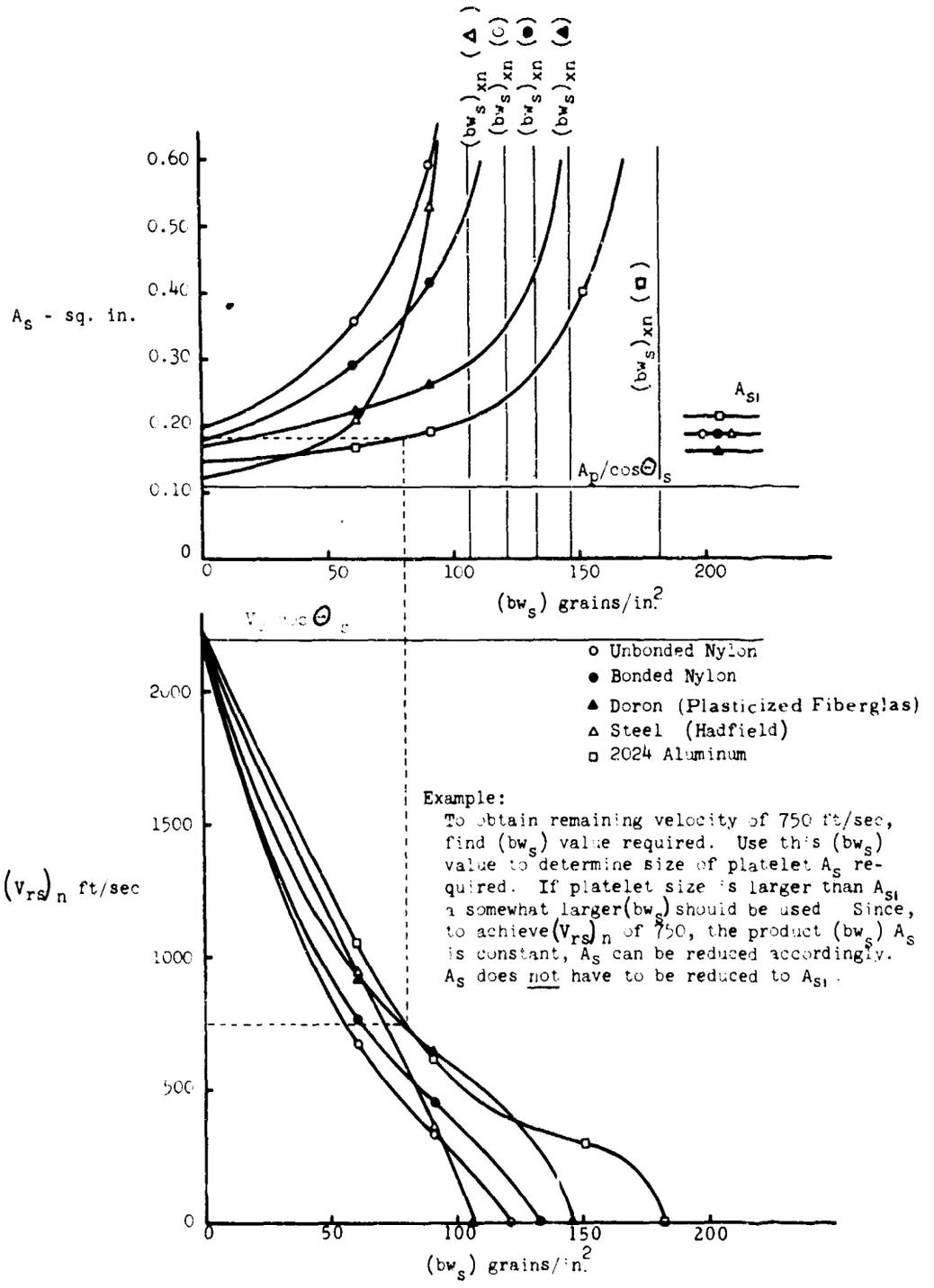

Figure 19. Platelet Area and Remaining Velocity as a Function of Platelet Area Density

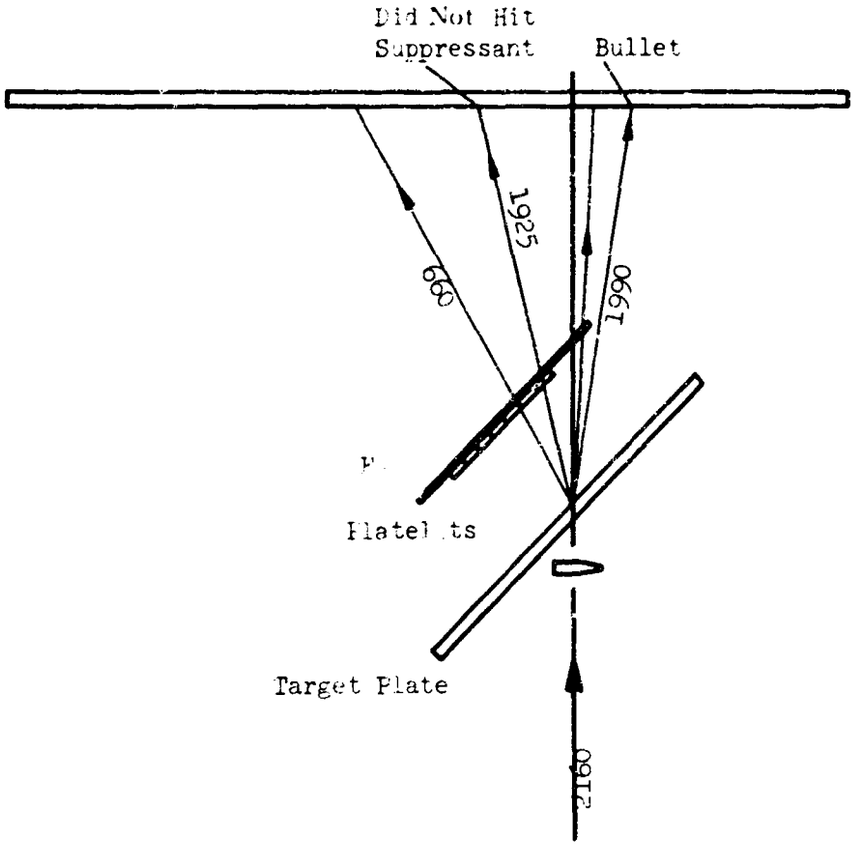

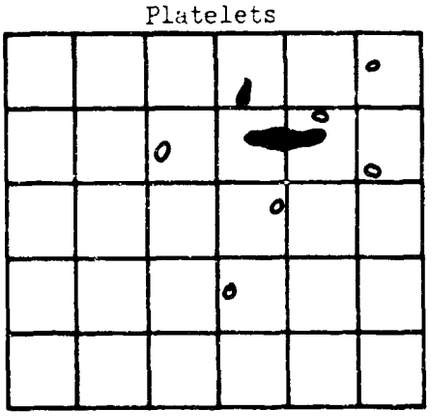

Figure 20. Diagram of Suppressant Test No. 202

Figure 21. Close-Up of Gun and Impact Chamber Showing Velocity Measurement Circuits

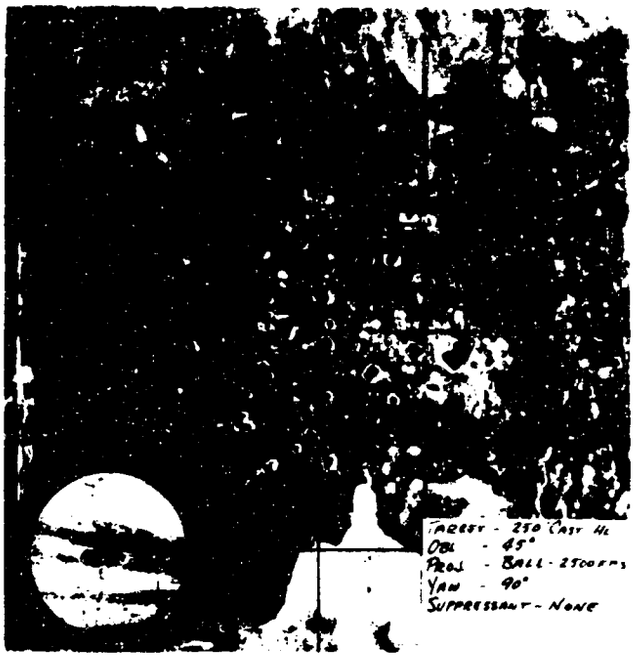

Figure 22. Witness Sheet Showing Results of Impact of Cast Aluminum Without Suppressant

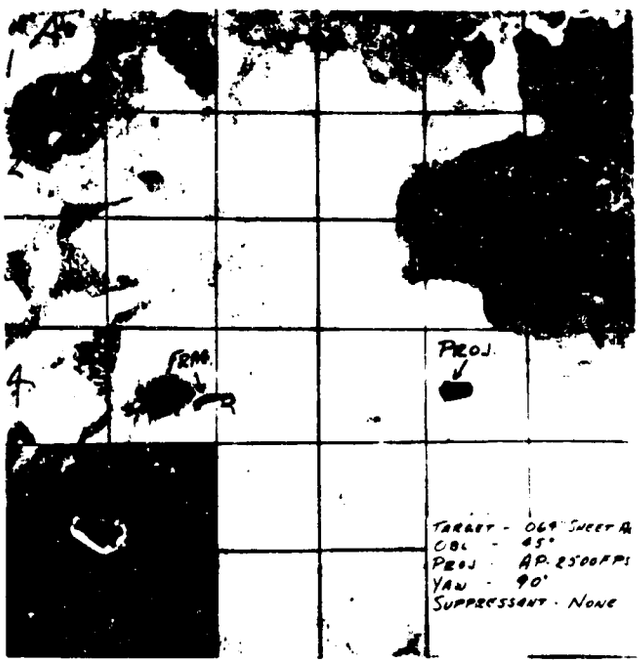

Figure 23. Witness Sheet Showing Results of Impact of Aluminum Sheet Without Suppressant

Figure 24. Witness Sheet Showing Results of Impact of Aluminum Sheet; Ionomer Suppressant in Contact

Figure 25. Witness Sheet Showing Results of Impact of Aluminum Sheet; Composite Suppressant in Contact

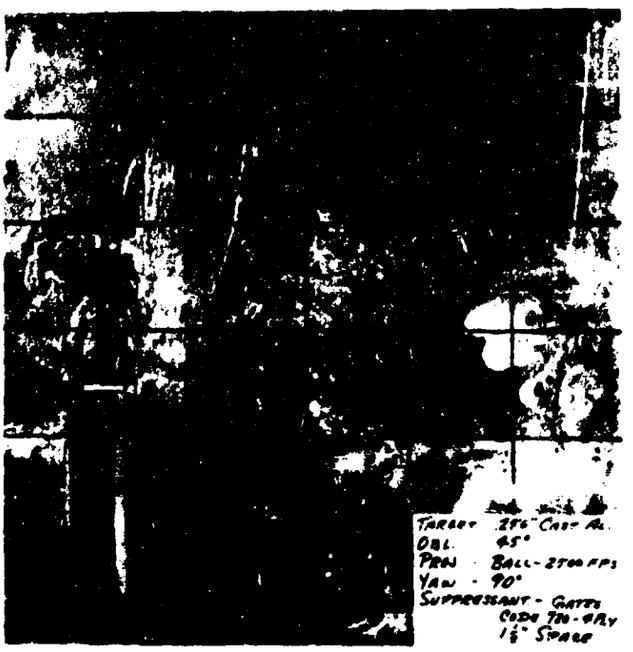

Figure 26. Witness Sheet Showing Results of Impact of Cast Aluminum Using Code 720 Suppressant 1-1/2 inches Behind Target

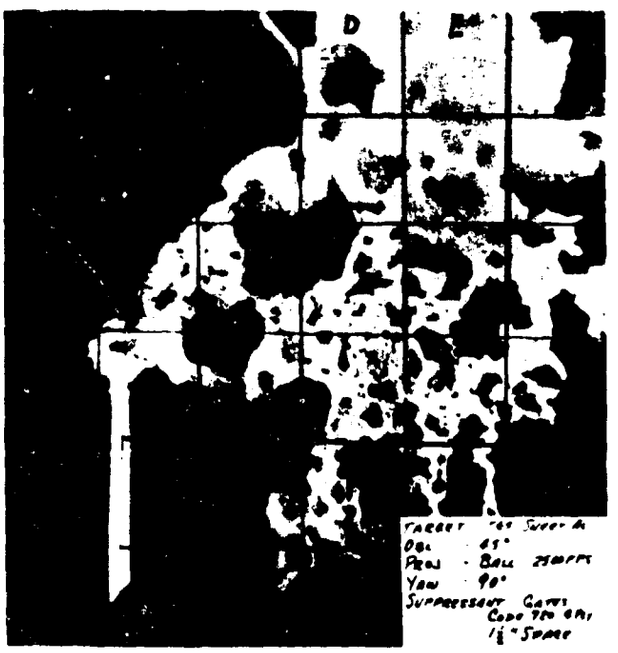

Figure 27. Witness Sheet Showing Results of Impact of Aluminum Sheet Using Code 720 Suppressant 1-1/2 inches Behind Target

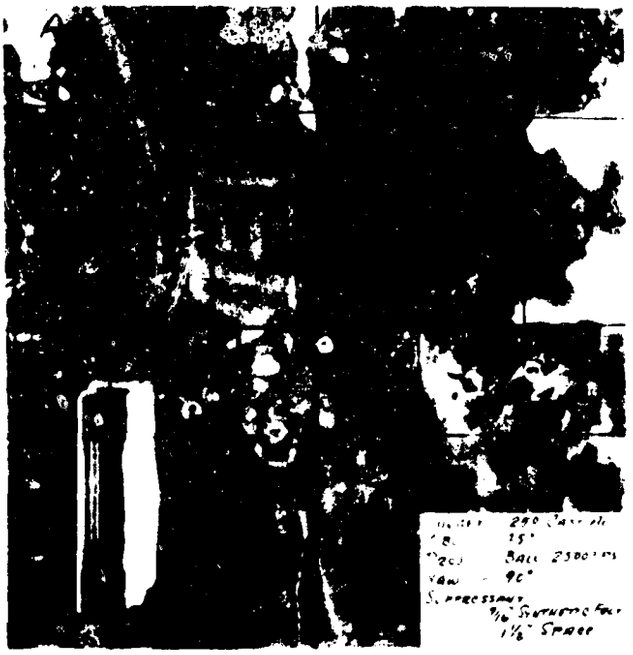

Figure 28. Witness Sheet Showing Results of Impact of Cast Aluminum Using Synthetic Felt Suppressant 1-1/2 inches Behind Target

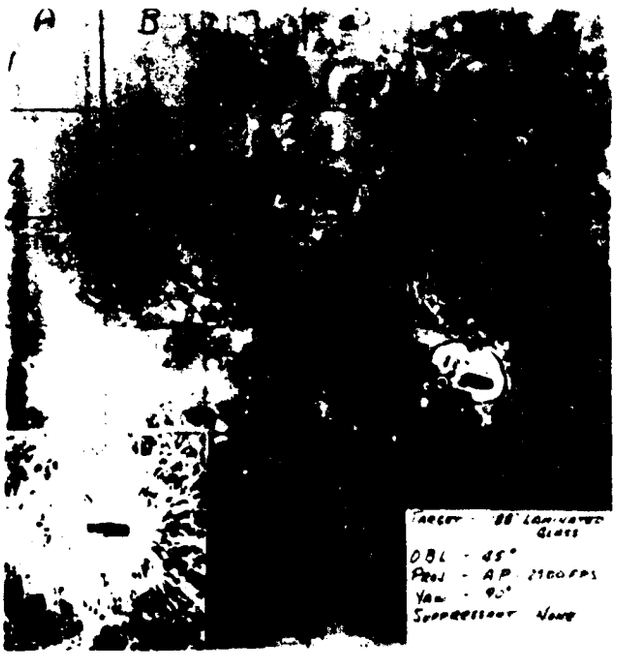

Figure 29. Witness Sheet Showing Results of Impact of Laminated Glass Without Suppressant

Figure 30. Witness Sheet Showing Results of Impact of Stretched Acrylic Plate Without Suppressant

Figure 31. Witness Sheet Showing Results of Impact of Laminated Glass Using Ionomer Sheet Suppressant

Figure 32. Comparison of Laminated Glass (Left) and Stretched Acrylic Plastic (Right) Impacted by Yawing Caliber .30 Projectile

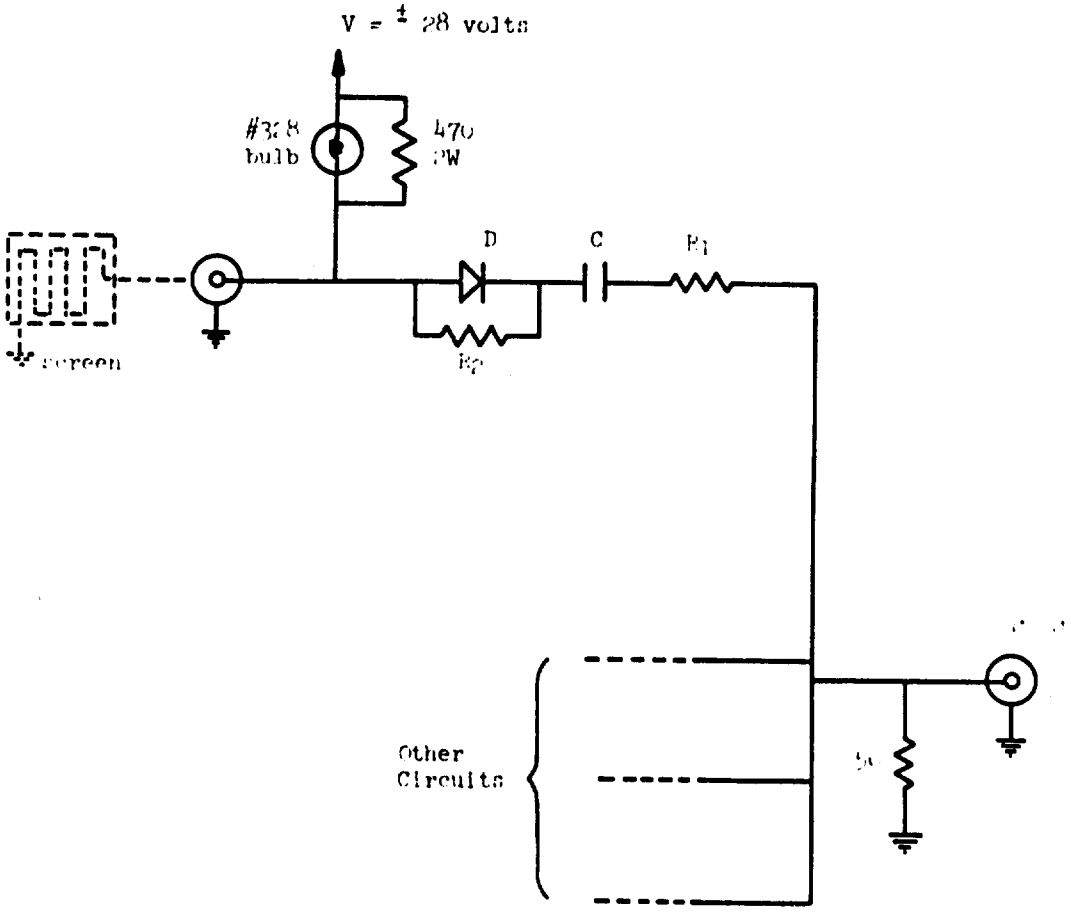

Figure 33. Typical Time-of-Arrival Circuit

Figure 34. Instrumentation Used To Obtain Records of Projectile and Fragment Velocities

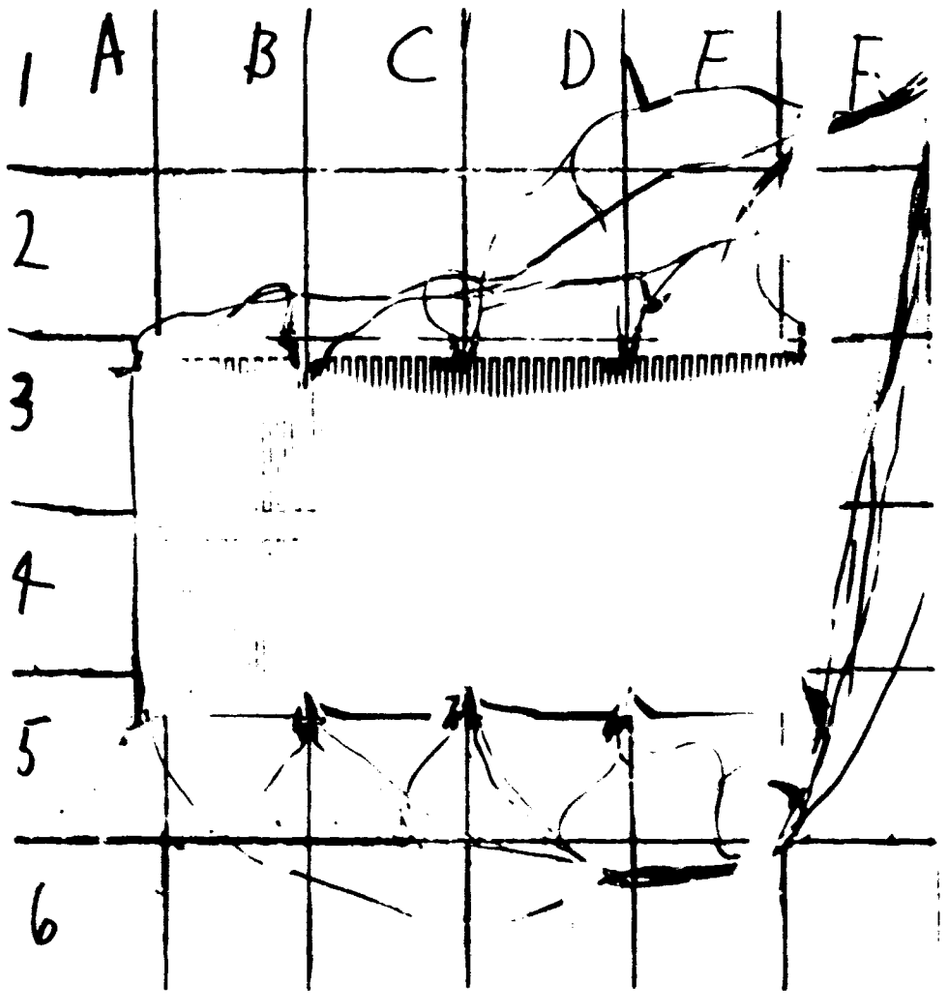

Figure 35. Celotex Backstop With Eight Conducting Circuits Attached

REFERENCES

1. R. F. Recht and T. W. Ipson, "Ballistic Perforation Dynamics", Trans. ASME, Journal of Applied Mechanics, September 1963.

2. Metallurgical Society Conferences, Response of Metals to High Velocity Deformation, Proceedings AIME Conference, July 11-12, 1960. Interscience Publishers, New York.

3. J. S. Rinehart, "Compilation of Dynamic Equation of State Data for Solids and Liquids", US NOTS TP 3798, Naval Ordnance Test Station, China Lake, California, May 1965.

4. Joseph Marin, Mechanical Behavior of Engineering Materials, Prentice-Hall, Inc., New Jersey, 1962.

5. W. James Lyons, "Impact Phenomena in Textiles", M.I.T. Press, Cambridge, Massachusetts, 1963.

6. Report of Visit to South Vietnam. Army Material Command Aircraft and Aircrew Armor Team, February 10 - March 21, 1965.

APPENDIX I

DESCRIPTION OF INSTRUMENTATION FOR FRAGMENT VELOCITY DETERMINATION

A determination of fragment velocities can be made if the time of arrival of the first fragment in each of a number of strategically located zones behind the target can be measured. To avoid the necessity for a large number of recording devices, a system of time-of-arrival circuits was devised to permit the recording of several zones on a single oscilloscope trace. An oscilloscope preamplifier permitting the time-shared use of four input channels at a 1-megacycle sampling rate provides a four-fold increase in recording capability over that available with a single-channel preamplifier.

The basic circuit is shown in Figure 25, and recording instrumentation is shown in Figure 26. A break screen, shown dotted at the end of a length of coaxial cable in Figure 25, provides the time-of-arrival indication. The screen consists of a zig-zag pattern of conducting ink on paper backing (see Figure 27). In operation, a current of approximately 0.1 amp is supplied to the screen through a No. 328 lamp and a 470-ohm resistor in parallel. The lamp provides visual evidence of circuit continuity before a test. Since the resistance of the screen is about 50 ohms, the voltage at the junction of the lamp and screen is about 5 volts. The supply voltage is 24 volts and may be positive or negative, depending upon whether the desired output pulse is positive or negative.

When a fragment penetrates the screen, the circuit is interrupted and the voltage at the junction of the lamp and screen rises toward the supply voltage. The rise time of the circuit depends upon the length of cable between the circuit and the screen. For 30-foot cables, the time constant involved is less than 1 microsecond and may be neglected for the present application. This fast-rising step is coupled through the diode, D, to the differentiating network consisting of R_1, C, and the 50-ohm load resistor. The pulse appearing at the output connector is attenuated by the divider, consisting of the load resistor and R_1, to a value of the order of 1 volt. The exact amplitude is determined by the value of R_1, and the shape (decay time constant) is determined by the values of R_1 and C. By varying the sizes of R_1 and C, pulses of several amplitudes and shapes can be developed and fed to a common load resistor and output line, as illustrated in Figure 6. In theory,

it should be possible to add as many as 16 different pulses to a single output line; i.e., four different time constants, two amplitudes and both polarities. However, for the present program it was decided to limit the number of pulses per output to four to facilitate data reduction. Thus, a total of 16 screens could be recorded with a four-channel pre-amplifier.

The diode, D, is included to prevent multiple triggering at a given screen. Once a screen has been broken long enough for the differentiating network to discharge, it must be closed for a time determined by the time constant of R_2 and C, before a second pulse can be generated. The resistor, R_2, is made much larger than R_1 to insure that a second pulse does not appear during the time of interest.

APPENDIX II

SUMMARY OF TEST DATA

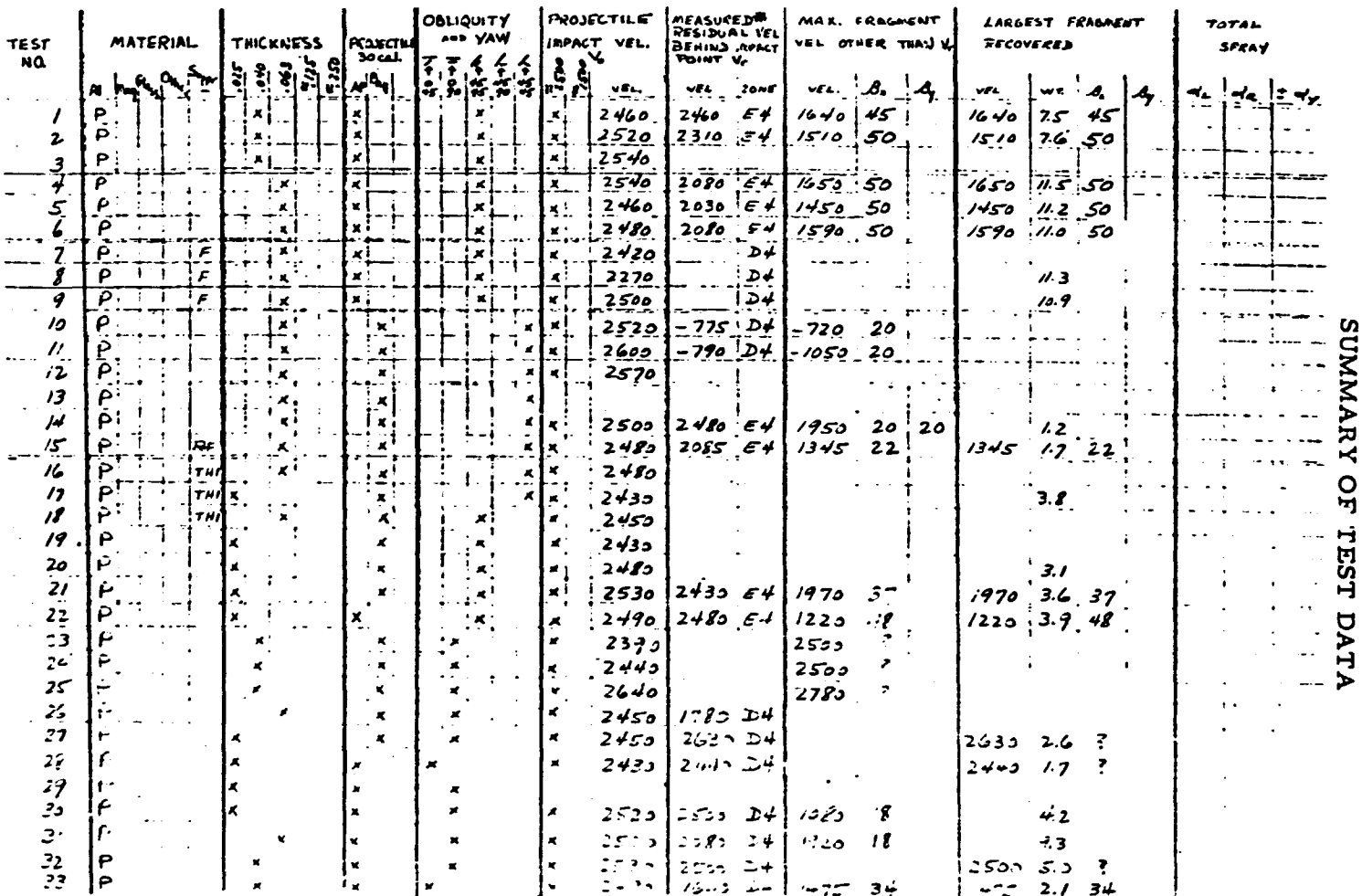

TEST NO.	MATERIAL	THICKNESS	PROJECTILE .30 cal.	OBLIQUITY AND YAW	PROJECTILE IMPACT VEL.	MEASURED RESIDUAL VEL BEHIND IMPACT POINT		MAX. FRAGMENT VEL OTHER THAN V_r			LARGEST FRAGMENT RECOVERED				TOTAL SPRAY			
					VEL.	VEL	ZONE	VEL.	B_0	A_f	VEL	WT	B_0	A_f	Φ_L	Φ_R	$\pm\Phi_V$
1	P				2460	2460	E4	1640	45		1640	7.5	45				
2	P				2520	2310	E4	1510	50		1510	7.6	50				
3	P				2540												
4	P				2540	2080	E4	1650	50		1650	11.5	50				
5	P				2460	2030	E4	1450	50		1450	11.2	50				
6	P				2480	2080	E4	1590	50		1590	11.0	50				
7	P	F			2420		D4										
8	P	F			2270		D4					11.3					
9	P	F			2500		D4					10.9					
10	P				2520	-775	D4	-720	20								
11	P				2600	-790	D4	-1050	20								
12	P				2570												
13	P																
14	P				2500	2480	E4	1950	20	20		1.2					
15	P	RF			2480	2085	E4	1345	22		1345	1.7	22				
16	P	THF			2480												
17	P	THF			2430							3.8					
18	P	THF			2450												
19	P				2430												
20	P				2480							3.1					
21	P				2530	2430	E4	1970	37		1970	3.6	37				
22	P				2490	2480	E4	1220	48		1220	3.9	48				
23	P				2390			2530	?								
24	P				2440			2500	?								
25	P				2640			2780	?								
26	P				2450	1780	D4										
27	P				2450	2620	D4				2630	2.6	?				
28	P				2430	2410	D4				2400	1.7	?				
29	P																
30	P				2520	2530	D4	1020	18			4.2					
31	P				2510	2080	D4	1120	18			4.3					
32	P				2530	2530	D4				2500	5.0	?				
33	P				2540	1610	D4	1475	34		1475	2.1	34				

CODE: P PLATE W WIPE I INTERLAYSHIT TH TEFLHIDE
C CASTING S SAFETY F FELT V VINYL
L PORTING K PLEXIGLAS R RUBBER

* It may be projectile or fragment

TEST NO.	MATERIAL	THICKNESS	PROJECTILE 30 cal.	OBLIQUITY AND YAW	PROJECTILE IMPACT VEL.	MEASURED * RESIDUAL VEL BEHIND IMPACT POINT V_r		MAX. FRAGMENT VEL. OTHER THAN V_r			LARGEST FRAGMENT RECOVERED				TOTAL SPRAY		
	Al Mag Fluor Other Steel	.025 .040 .063 .125 .250	AP B_{AP}	0° ±45° 30° ±45° 45° ±45° 60° ±45° 75° ±45°	1100 1200 VEL.	VEL	ZONE	VEL	B_a	B_y	VEL	WT.	B_a	B_y	d_L	d_z	$\pm d_y$
34	P	×	×	×	×	2530	2270	D4	2090	18		1680	4.2	34				
35	P	×	×	×	×	2500	2500	D4	2080	19		2080	1.4	19				
36	P	×	×	×	×	2490	2440	D4	2170	19		2170	2.0	19				
37	P	×	×	×	×	2470	2330	D4	2130	19		2130	2.6	19				
38	P	×	×	×	×	2650	2330	D4	2080	19		2080	3.0	19				
39	W		×	×	×	2370												
40	W		×	×	×	2500	1880	D4	1830	19								
41	P	1 2	×	×	×	2250	2180	D4	1650	19		1650	3.0	19				
42	P	1 2	×	×	×	2500	2440	D4	2000	19			2.7	19				
43	P	(.032) 1 2	×	×	×	2290	2170	D4					7.4					
44	P	(.039) 1 2	×	×	×	2560	2330	D4	2280	19								
45	P	(.049) 1 2	×	×	×	2530	2280	D4	1710	19								
46	P	(.039) 1 2	×	×	×	2940	1750	D4	2000	22		1620	2.4	29		30	18	23
47	P	1 2	×	×	×	2300	2040	D4	1785	16	3	1785	5.4	16	3	21	24	27
48	P	1 2	×	×	×	2570	2450	D4	1810	28	6	1810	1.8	28	6			
49	P	(.049) 1 2	×	×	×	2340	2180	D4	1865	20	7	1865	9.8	20	7	22	13	22
50	P	1 2	×	×	×	2380	2220	D4	2040	16	3	2040	2.6	16	3	22	9	39
51	P	1 2	×	×	×	2500	2500	D4										
52	P	2 1	×	×	×	2490	2340	D4	1350	3	11		2.6			22	9	39
53	P	(.032) 2 1	×	×	×													
54	P	(.039) 2 1	×	×	×	2460	2330	D4	1320	5	18	1320	0.8	5	18	18	10	63
55	P	(.032) 2 1	×	×	×	2460	2380	D4	1760	3	15	1760	2.2	3	15	26	12	39
56	P	(.032) 2	×	×	×	2480	2330	D4	1820	4	13		9.8			11	17	34
57	P	(.032) 2	×	×	×	2440	2220	D4					13.7			12	3	20
58	P	1 2	×	×	×	2420	2330	D4	1360	3	32							36
59	P	×	×	×	×	2590	2510	E4	2400	14		2400	9.4	14		41	10	41
60	P	×	×	×	×	2500	2250	E4	1800	33		1800	8.7	33		54	8	50
61	P TH	×	×	×	×	2445	2190	E4	1480	32	9	1480	2.9	32	9	47	9	50
62	P TH	×	×	×	×	2690												
63	P TH	×	×	×	×	2800	2320	E4	1535	6		1535	3.2	6		43	16	16
64	P	(.032) 2	×	×	×	2700	2610	E4	1790	39		1790	13.4	39		47	15	43
65	P P	×	×	×	×	2600	2520	E4	1745	36	2	1745	5.0	36	2	44		45
66	P	×	×	×	×	2440												

D-Dynafax Photo
F-Fastax Photo

□ Platelet
C CASTING
CE CELOTEX
CG CAST GUN MOUNT
CH CHECKSTRAP
CO COTTON
E ESTANE
F FELT
FG FIBERGLAS
G GATES CODE 960
I INSTRUMENT
L LEXAN
P PLATE
PE POLYETHYLENE
PV POLYVINYL
R RUBBER
S SAFETY
SU SURLYN
T TUBING
TB TENITE BUTYRATE
TH TEX-HIDE
V VINYL
W WIRE
X PLEXIGLAS

*May be projectile or frag.

TEST NO.	MATERIAL	THICKNESS	PROJECTILE 30 cal.	OBLIQUITY AND YAW	PROJECTILE IMPACT VEL.	MEASURED RESIDUAL VEL BEHIND IMPACT POINT V_r		MAX. FRAGMENT VEL. OTHER THAN V_r				LARGEST FRAGMENT RECOVERED				TOTAL SPRAY		
						VEL.	ZONE	VEL.	B_L	A_y		VEL.	WT.	B_L	A_y	$\pm d_L$	$\pm d_z$	$\pm d_y$
67	P				2450													
68	P	1 2			2530	2520	E4	1685	46			1685	8.5	46				
69	P				1460	1330	E4											
70	P				1390	1295	E4									12	6	6
71	P				1380	1330	E4									9	9	3
72	P				1560	1500	E4	1400	18	2			1.9			30	6	3
73	P				1525	1390	E4	1490	19			1490	10.4	19			19	
74	P				1000													
75	P	1 2			2320	1865	E4	1950	20			1950	11.4	20				
76	P	1 2			2510													
77	P	1 2			2620													
78	P	1 2			2600													
79	C				2560		E4	2105	19	7		1685	3.7	27	2	50	15	36
80	C				2510	1655	E4	1810	26			1780	9.4	27	15	47	10	36
81	C				2500	2180	E4	2280	12	8						50	10	34
82	C				2590	2180	D4	2180	11	10						44	5	34
83	C C				2570	2080	E4	1885	15	5		1360	12.6	45		52	10	32
84	C C				2620	1920	D4	1820	19	12		1600	3.5	23	3	44	20	41
85	C				2600	2280	E4	2200	33	5		2200	2.8	33	5	50	5	39
86	C C				2520											50		39
87	C C				2515	1820	E4	2060	25	3		2060	2.6	25	3	50	5	43
88	C C	R-F			2530	1780	E4	1940	24	6		1940	3.7	24	6	50	5	36
89	C C				2500								6.4			56	10	42
90	C C				2535	1880	E4	1910	25	8						52	22	38
91	C C												13.2			49	19	44
92	C				2590	2120	E4	1790	21	6		1440	5.5	34	18	42	19	40
93	C C				2545	2310	E4	2260	39	3						50	5	39
94	C C				2790	2220	E4	2660	25	3						54	15	34
95	C C				2500	2330	E4	2150	36	5						47	10	39
96	C C															52	10	39
97	C C				2525	2080	E4	2290	21	9						54	11	42
98	C				2500	2060	E4	2360	10							49	20	42
99	C				2480	1960	E4	2050	30	12								

CODE: P PLATE, C CASTING, T TURNING, W WIRE, S SAFETY, X PLEXIGLAS, I INSTRUMENT, F FELT, R RUBBER, TH TEX-HIDE, V VINYL

* may be projectile or fragment

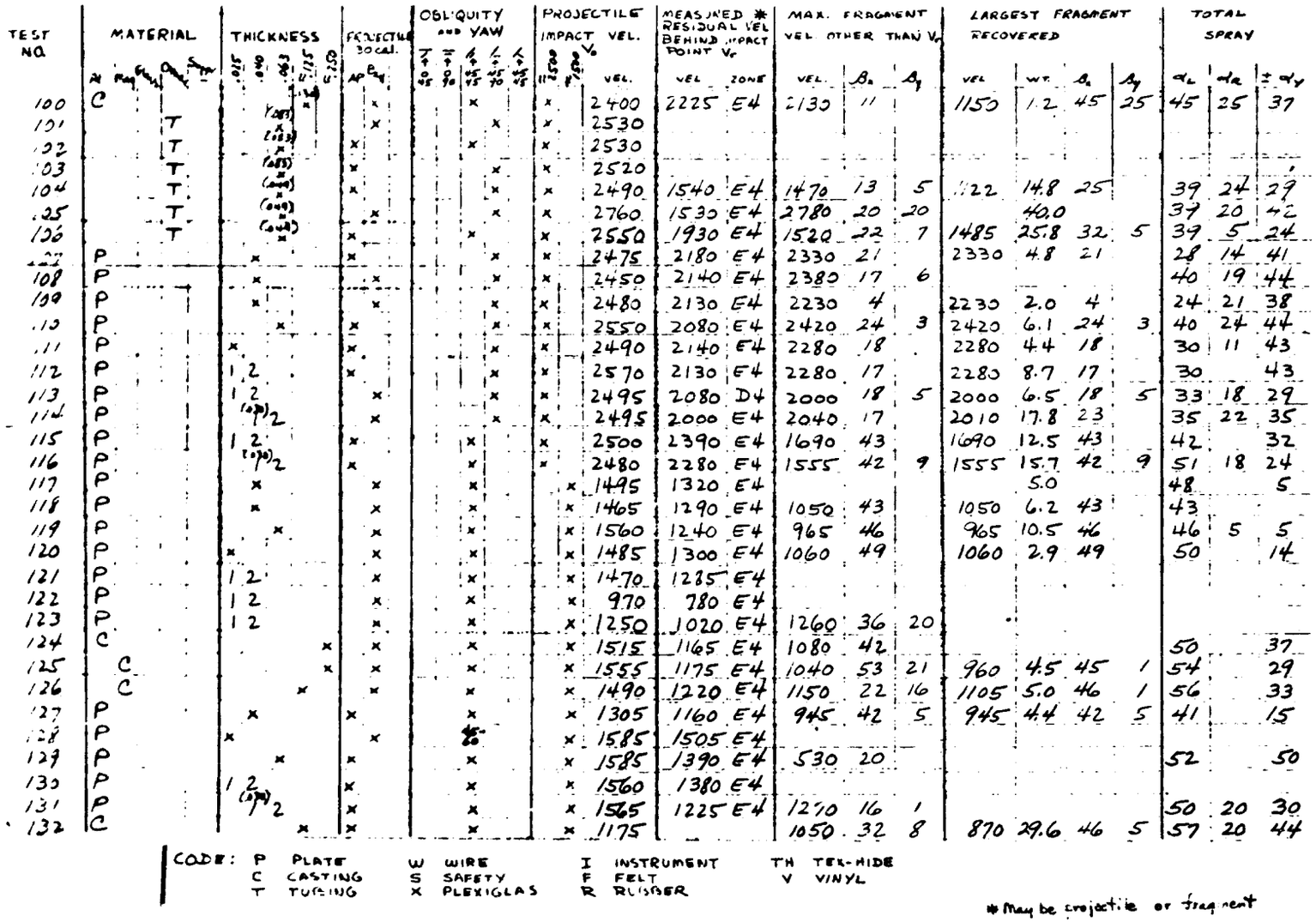

TEST NO.	MATERIAL	THICKNESS	PROJECTILE .30 CAL.	OBLIQUITY AND YAW	PROJECTILE IMPACT VEL. V_o	MEASURED * RESIDUAL VEL BEHIND IMPACT POINT V_r		MAX. FRAGMENT VEL OTHER THAN V_r			LARGEST FRAGMENT RECOVERED				TOTAL SPRAY		
					VEL.	VEL	ZONE	VEL.	β_x	β_y	VEL	WT.	β_x	β_y	α_L	α_R	$\pm\alpha_Y$
100	C				2400	2225	E4	2130	11		1150	1.2	45	25	45	25	37
101	T				2530												
102	T				2530												
103	T				2520												
104	T				2490	1540	E4	1470	13	5	1122	14.8	25		39	24	29
105	T				2760	1530	E4	2780	20	20		40.0			37	20	42
106	T				2550	1930	E4	1520	22	7	1485	25.8	32	5	39	5	24
107	P				2475	2180	E4	2330	21		2330	4.8	21		28	14	41
108	P				2450	2140	E4	2380	17	6					40	19	44
109	P				2480	2130	E4	2230	4		2230	2.0	4		24	21	38
110	P				2550	2080	E4	2420	24	3	2420	6.1	24	3	40	24	44
111	P				2490	2140	E4	2280	18		2280	4.4	18		30	11	43
112	P	1 2			2570	2130	E4	2280	17		2280	8.7	17		30		43
113	P	1 2			2495	2080	D4	2000	18	5	2000	6.5	18	5	33	18	29
114	P	$(2P)_2$			2495	2000	E4	2040	17		2010	17.8	23		35	22	35
115	P	1 2			2500	2390	E4	1690	43		1690	12.5	43		42		32
116	P	$(2P)_2$			2480	2280	E4	1555	42	9	1555	15.7	42	9	51	18	24
117	P				1495	1320	E4					5.0			48		5
118	P				1465	1290	E4	1050	43		1050	6.2	43		43		
119	P				1560	1240	E4	965	46		965	10.5	46		46	5	5
120	P				1485	1300	E4	1060	49		1060	2.9	49		50		14
121	P	1 2			1470	1285	E4										
122	P	1 2			970	780	E4										
123	P	1 2			1250	1020	E4	1260	36	20							
124	C				1515	1165	E4	1080	42						50		37
125	C				1555	1175	E4	1040	53	21	960	4.5	45	1	54		29
126	C				1490	1220	E4	1150	22	16	1105	5.0	46	1	56		33
127	P				1305	1160	E4	945	42	5	945	4.4	42	5	41		15
128	P				1585	1505	E4										
129	P				1585	1390	E4	530	20						52		50
130	P	1 2			1560	1380	E4										
131	P	$(2P)_2$			1565	1225	E4	1270	16	1					50	20	30
132	C				1175			1050	32	8	870	29.6	46	5	57	20	44

CODE: P PLATE, C CASTING, T TUFFING; W WIRE, S SAFETY, X PLEXIGLAS; I INSTRUMENT, F FELT, R RUBBER; TH TEK-HIDE, V VINYL

* May be projectile or fragment

TEST NO.	MATERIAL	THICKNESS	PROJECTILE .30 cal.	OBLIQUITY AND YAW	PROJECTILE IMPACT VEL.	MEASURED * RESIDUAL VEL BEHIND IMPACT POINT V_r		MAX. FRAGMENT VEL. OTHER THAN V_r			LARGEST FRAGMENT RECOVERED				TOTAL SPRAY		
					VEL.	VEL	ZONE	VEL.	B_x	A_y	VEL.	W_R	B_x	A_y	d_L	d_x	$\pm d_y$
133	C		x	x	1555	1380	E4	1050	31	5	945	1.6	43	10	53	15	39
134	C		x	x	1525	1090	E4	865	36	3	690	3.5	23	28	53		39
135	C		x	x	1570	1100	E4	1155	16	17	1070	6.2	40	4	52		40
136	C		x	x	1575	1390	E4	1440	23	4	990	0.8	28	12	56	5	29
137	C		x	x	2460	1725	D4	1785	34								
138	C		x	x	2460										44		40
139	C		x	x	2540										34	27	40
140	S	.119		x	580	2325	D4	1825		18							
141	P		x	x	2480	1885	D4	1610		18							
142	P		x	x	2560	2000	D4	1820		18							
143	S	.119		x	2460												
144	S	.119		x	2500												
145	X		x	x	2500	1175	E4	1280	39		1280	4.4	39		54	10	31
146	X		x	x	2480												
147	X		x	x	2540	1990	E4	2260	36						56	10	36
148	X		x	x	1685	1275	E4	1540	47	20					54	15	33
149	X	.118		x	2440	2080	E4	2170	36						54	10	39
150	S		x	x	2540										53	10	24
151	X		x	x	2680	2290	E4	2000	7		1360	4.3	36		48	5	15
152	X	PV	x	x	2600							1.4			50	29	10
153	X	.119		x	2680	2350	E4	1990	47		1990	3.8	47		56		32
154	X	E		x	2580	2400	D4	1640	19						52	5	30
155	X	SU		x	2540	2230	E4	2080	36						41	5	5
156	X	V		x	2610	2500	D4										
157	S	V		x	2540	2130	D4	1450	49						49		3
158	S		x	x	2580	2040	E4	2080	18						54	12	27
159	X	V		x	-	2500	E4	1810	46		1810	3.8	46		46		2
160	S	V		x	-	2180	E4	1960	18						49	9	12
161	P			x	2480	1754	E4	1785	21						58	16	30
162	S	V		x	2500	2080	E4	1880	17						49	4	21
163	S		x	x	2680	2260	E4	1750	46						50	12	27
164	X		x	x	2520	2290	E4	2180	20	20	2050	5.2	48		54	15	36
165	C	TH	x	x	2520	2040	E4	1580	38						30	21	34

CODE: P PLATE, C MATING, — FOLDING, W WIRE, S SAFETY, X PLEXIGLAS, I INSTRUMENT, F FELT, R RUBBER, TH TEL-HIDE, V VINYL

* May be projectile or fragment

TEST NO.	MATERIAL	THICKNESS	PROJECTILE	OBLIQUITY AND YAW	PROJECTILE IMPACT VEL. V_o	MEASURED* RESIDUAL VEL BEHIND IMPACT POINT V_r		MAX. FRAGMENT VEL OTHER THAN V_r			LARGEST FRAGMENT RECOVERED				TOTAL SPRAY		
					VEL.	VEL	ZONE	VEL	B_o	A_f	VEL	WT.	A_o	A_f	α_L	α_a	$\Sigma\alpha_y$
166	C P				2650	2040	D4	1890		20					32	10	24
167	P P				2680	2290	D4	2420		20							
168	P P			45° 60°	2540	1990	E4	2130	20						29	10	20
169	P P			45°	941	602	E4										
170	P P				1322	982	D4	1020	20								
171	P P				1220												
172	P P				1240												
173	P P				1420	1223	D4	1348	7	10		4.7			7	16	39
174	P P				1600	1175	E4	1235	16		1235	10.5			16		
175	P P				1430	972	E4	1225	20		708	12.6	19	24	3	19	24
176	P P				1460							1.1				8	21
177	P P				2560	2670	E4								10	15	29
178	P P				2590	2415	E4								10	15	29
179	C P				2635	2018	E4	2135	3		2125	4.0	27	10	45	20	36
180	C P				2540	2330	D4	2375	10						38	16	23
181	P P				2705	2500	D4	2085	23	2	2085	1.0	23	2	25		23
182	P P				2500	-	E4	2410		20	1790	3.7	33		47	19	35
183	CG P	.175		45° 35°	2670	2300	E4	1900	35	2	-	5.5	40	35	55	11	36
184	CG P	.175			2460	1905	E4	1770	44		1770	5.5	44		54	5	31
185	CG P	.175			2530	2090	E4	1830	13	2	1720	9.8	42	24	53	18	33
186	CG P	.175			2730	2330	D4	2090	22	9	2090	2.2	22	9	40	18	35
187	P P			0-0	2920	2440	D4								5	2	7
191	C P	.175		0-0	2680	2500	D4								5	2	7
54	C P	AL .063			3220	2290	E4	1110	41		1110	9.1	41		46		10
73	P P	AL .040		45° 60°	2490	2290	E3	2090	7	3	1555	10.3	34	2	42		27
91	P P	AL .040			2500	2180	E4	1760	3	4	1460	5.6	32		51		31
192	P P	AL .040			2610	2340	E4	2520	8	2	2440	4.3	24	1	37	5	27
193	P P	AL .063			2480	—									24	24	22
194	P P □	AL .040			2480	1970	E4	2280	12	1	950	5.0	30	2	37	16	40
195	P P □	AL .040			2480	2130	E4	2360	33	2	2360	4.3	33	2	49	10	33
196	P P □	AL .040			2505	2180	E4	2330	21		2330	4.3	21		44	5	36
197	P P	TH .040			2545	2240	E4	2130	20	2	940	2.7	29	2	50	8	33
198	P P	TH .040			2445	2080	D4	1890	24	8	1890	1.0	24	8	24	8	31

□ PLATELET

CODE: P PLATE, C CASTING, T TURNING, CG CAST GUN MOUNT, W WIRE, S SAFETY, X PLEXIGLAS, I INSTRUMENT, F FELT, R RUBBER, TH TEL-HIDE, V VINYL

* may be projectile or fragment

TEST NO.	MATERIAL			THICKNESS				PROJECTILE .30 CAL.	OBLIQUITY AND YAW					PROJECTILE IMPACT VEL.	MEASURED* RESIDUAL VEL BEHIND IMPACT POINT V_r		MAX. FRAGMENT VEL OTHER THAN V_r			LARGEST FRAGMENT RECOVERED				TOTAL SPRAY		
	N													VEL.	VEL	ZONE	VEL.	B_0	A_f	WT.	WT.	A_r	A_f	n_r	n_f	Σn_f
199	P		TH2		X			X			X		X	2540	2230	E4	2250	19	3	1790	7.5	21	2	37	17	26
200	C		TH2				X	X			X		X	2500	1475	E4	1670	6	4	—	5.8			38	12	30
201		T	TH2	.249			X			X			X	2890	1725	D4	1505	4	4					21	23	30
202	P		TH2		X			X			X		X	2610	1590	E4	1925	16	16	660	3.0	28	1	46	8	27
203	P	□	TH2		X			X			X		X	2680	2180	E4	2400	39	36	2250	0.6	13	8	34	13	31
204	P	□	TH2		X			X			X		X	2880	2280	E4	2440	5	3					48	13	27
205	P		TH2		X			X		X			X	2880	2290	E4								31		5
206	P		TH2		X			X			X		X	2700	2290	E4	2270	23	1	2000	1.3	11	13	41	5	22
207	P		TH2		X			X			X		X	2420	1980	E4	2080	5								
208	P		TH2		X			X			X		X	2540	1875	E4	1990	8						45	8	28
209	P		TH2	X				X			X		X	2700	2230	E4	2310	16	7					37	10	26
210	P		TH2		X			X			X		X	2570	1950	E4	2010	13	6	1950	4.1	11	3	46	15	24
211	P		TH2		X			X		X			X	2590	2130	E4	2120	10	5	2040	-			49	6	27
212	P		TH2		X			X		X			X	2660	2340	E4	2360	8	2					42	10	24
213	P		TH2		X			X		X			X	2480	2090	E4	2040	9						38	6	22
214	P		TH2		X			X		X			X	2480	2080	E4	2130	29	3					45	8	33
215	P		TH2		X			X			X		X	2500	2090	E4	2280	5	2					10	8	15
216	C		CH2			X		X			X		X	2480	—									41	22	29
217	P		CH2		X			X			X		X	2480	1025	E4	990	12	12					46	-	21
218	P		CG2		X			X			X		X	2420	1855	E4	1925	12						33	19	21
219	P		TH2		X			X			X		X	2500	1840	E4	1960	15		1960	4.4	15		41	12	28
220	P		TH3		X			X			X		X	2440	1865	E4	1835	4						32	20	31
221	P		CG2		X			X			X		X	2350	1910	E4	1740	11	6					13	20	20
222	C		CG2			X		X			X		X	2500	1145	E4	735	4	4					29	10	18
223		T	GB	.249				X			X		X	2520	910	E3	485	17	13					17	19	35
224	P		GL		X			X			X		X	2520	-		-							36	18	22
225	P		G4		X			X			X		X	2620	—		—							20	13	15
226	P		G1		X			X			X		X	2540	1990	E4	2030	9						31	20	24
227	P		G1		X			X			X		X	2650	2280	E4	2310	20	20					20	10	20
228	P		G1		X			X			X		X	2500	2290	E4	2230	9		1265	6.0	25		34	10	22
229	P		G4		X			X			X		X	2520	190[illegible]	E4	2130	19								
230	P		G2		X			X			X		X	2500	20[illegible]	E4	2220	19		1339	6.2	27				
231	C		G4			X		X			X		X	2460	530	E4	1295	19								

CODE: P PLATE W WIRE I INSTRUMENT TH TEL-HIDE
C CASTING S SAFETY F FELT V VINYL
T TUBING K PLEXIGLAS R RUBBER

* May be projectile or fragment

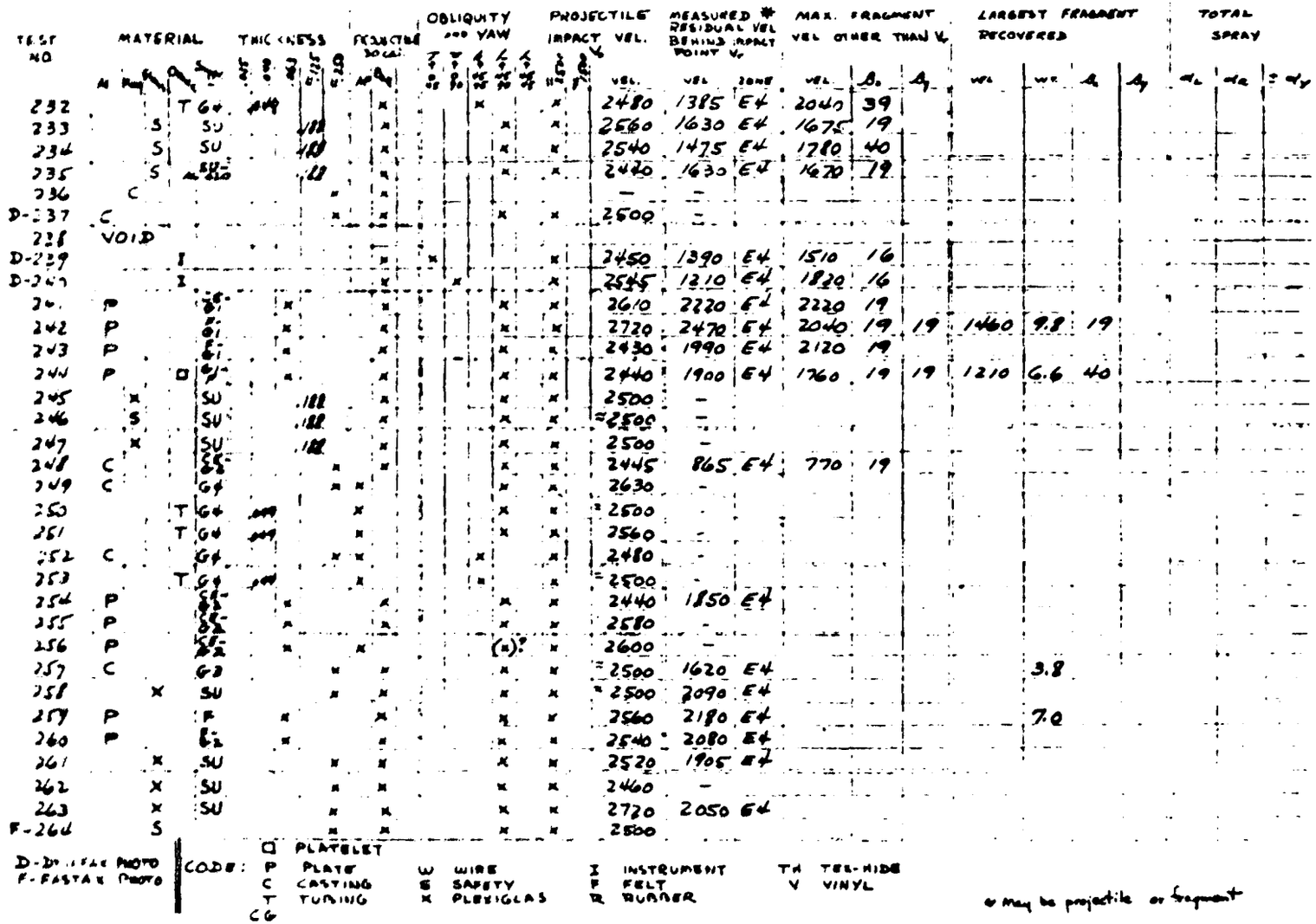

TEST NO	MATERIAL	THICKNESS	PENETRATE 30 CAL	OBLIQUITY AND YAW	PROJECTILE IMPACT VEL.	MEASURED * RESIDUAL VEL BEHIND IMPACT POINT V_r		MAX. FRAGMENT VEL OTHER THAN V_r			LARGEST FRAGMENT RECOVERED				TOTAL SPRAY		
						VEL.	ZONE	VEL	B_o	A_y	VEL	WT.	B_o	A_y	σ_L	σ_a	σ_y
232	T G4	.249	X	X	2480	1385	E4	2040	39								
233	S SU	.188	X	X	2560	1630	E4	1675	19								
234	S SU	.188	X	X	2540	1475	E4	1780	40								
235	S SU	.188	X	X	2420	1630	E4	1420	19								
236	C		X	X	—	—											
D-237	C		X	X	2600	—											
238	VOID																
D-239	I		X	X	2450	1390	E4	1510	16								
D-240	I		X	X	2545	1210	E4	1820	16								
241	P		X	X	2610	2220	E4	2220	19								
242	P		X	X	2720	2470	E4	2040	19	19	1460	9.8	19				
243	P		X	X	2430	1990	E4	2120	19								
244	P □		X	X	2440	1900	E4	1760	19	19	1210	6.6	40				
245	X SU	.188	X	X	2500	—											
246	S SU	.188	X	X	2500	—											
247	X SU	.188	X	X	2500	—											
248	C		X	X	2445	865	E4	770	19								
249	C G4		X	X	2630	—											
250	T G4	.249	X	X	2500	—											
251	T G4	.249	X	X	2560	—											
252	C G4		X	X	2480	—											
253	T G4	.249	X	X	2500	—											
254	P		X	X	2440	1850	E4										
255	P		X	X	2580	—											
256	P		X	X	2600	—											
257	C G3		X	X	2500	1620	E4					3.8					
258	X SU		X	X	2500	2090	E4										
259	P		X	X	2560	2180	E4					7.0					
260	P		X	X	2540	2080	E4										
261	X SU		X	X	2520	1905	E4										
262	X SU		X	X	2460	—											
263	X SU		X	X	2720	2050	E4										
F-264	S		X	X	2500												

D-DIGITAL PHOTO
F-FASTAX Photo

CODE: □ PLATELET
P PLATE
C CASTING
T TUNING
CG
W WIRE
S SAFETY
X PLEXIGLAS
I INSTRUMENT
F FELT
R RUBBER
TH TEL-HIDE
V VINYL

* may be projectile or fragment

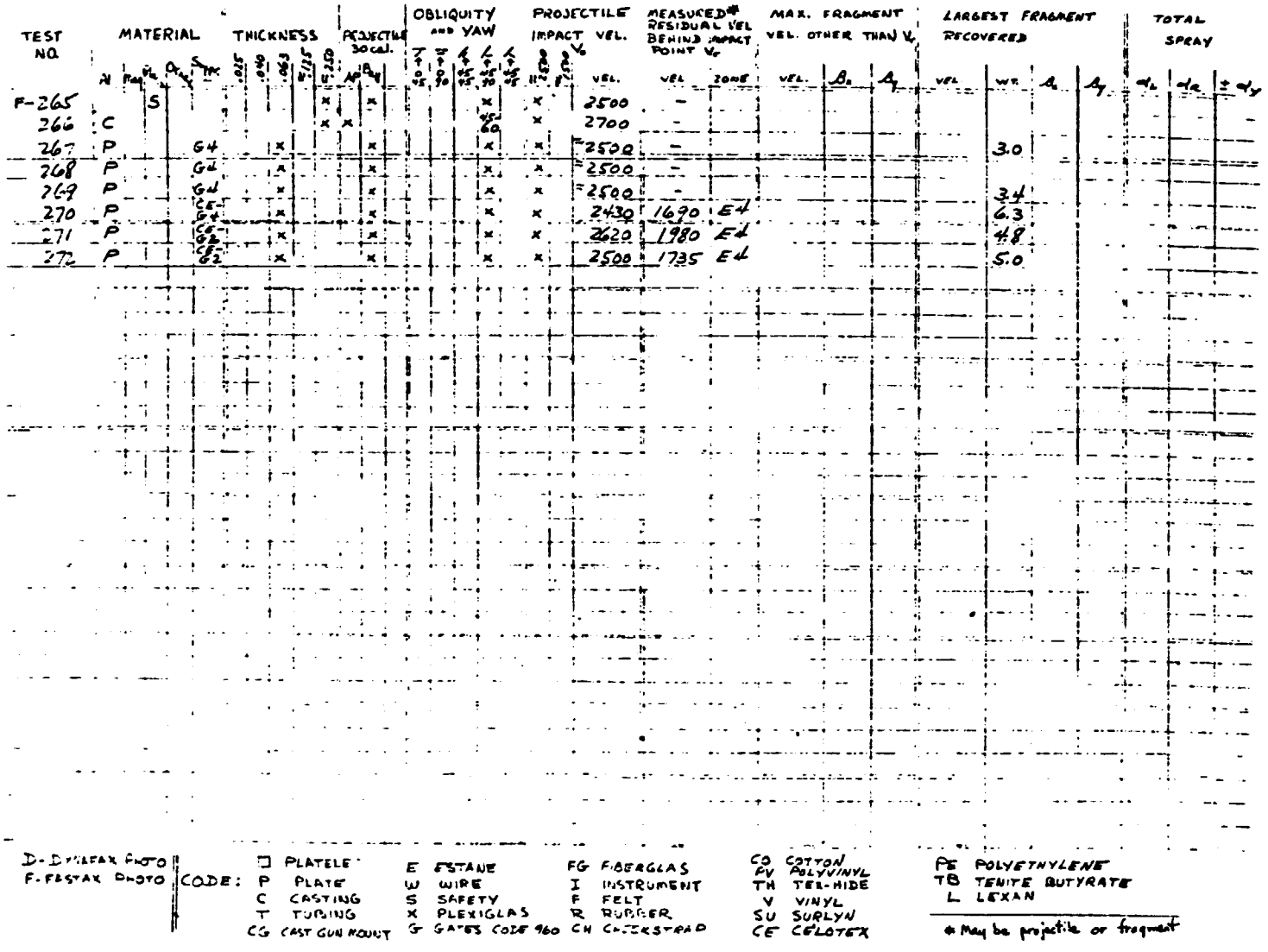
TEST NO.
MATERIAL
THICKNESS
PROJECTILE .30 cal.
OBLIQUITY AND YAW
PROJECTILE IMPACT VEL. V_o
MEASURED* RESIDUAL VEL BEHIND IMPACT POINT V_r
MAX. FRAGMENT VEL. OTHER THAN V_r
LARGEST FRAGMENT RECOVERED
TOTAL SPRAY
VEL.
ZONE
WT.
F-265 S 2500 -
266 C 2700 -
267 P G4 2500 - 3.0
268 P G4 2500 -
269 P G4 2500 - 3.4
270 P G4 2430 1690 E4 6.3
271 P G4 2620 1980 E4 4.8
272 P G4 2500 1735 E4 5.0
D-DuPont Photo
F-Fastax Photo
CODE: P PLATE, C CASTING, T TUBING, CG CAST GUN MOUNT, E ESTANE, W WIRE, S SAFETY, X PLEXIGLAS, G GATES CODE 960, FG FIBERGLAS, I INSTRUMENT, F FELT, R RUBBER, CH CHEESTRAD, CO COTTON, PV POLYVINYL, TH TEK-HIDE, V VINYL, SU SURLYN, CE CELOTEX, PE POLYETHYLENE, TB TENITE BUTYRATE, L LEXAN
* May be projectile or fragment

APPENDIX III

APPLICATION OF SUPPRESSANTS TO AIRCRAFT

Determination of areas within specific aircraft to which suppressants should be applied is beyond the scope of this program. It seems clear, however, that each area to be protected in each aircraft will have a unique installation problem for which a suppressant kit could be designed to provide maximum personnel protection from secondary fragments. The philosophy on which the design and installation procedures should be based is as follows:

1. Wherever possible, the suppressant should be applied directly to existing airframe structure (ribs, etc.) providing a normal standoff of 1-1/2 inches.

2. Suppressant should be attached to the airframe by a cement having a high bonding strength. (The airframe should not be modified, as by drilling.)

3. To the extent possible, the use of rivets, metal clips, etc., to attach suppressants to airframe should be avoided. Such devices become new sources of fragments.

4. Where special supports are required to obtain the desired standoff, such supports should be made of low-density materials incapable of producing hazardous fragments.

The cement used to bond the four-ply nylon suppressant to aircraft structural surfaces was EC1362. A tear test was conducted to establish the strength of the bond when this cement was used to adhere a sample of the four-ply nylon suppressant to a strip of aluminum. A force of 16 pounds per linear inch applied at a right angle to the joint was required to tear the material away from the aluminum.

Where the suppressant is to be used to cover a floor area in the aircraft and is required to support relatively heavy loads, the desired standoff may be achieved by use of foamed rubber or plastic padding such as that used under carpets in domestic applications. Impact tests were conducted to evaluate the effectiveness of the suppressant used in conjunction with padding of this type. A 1-1/2-inch-thick layer of

foamed rubber padding was sandwiched between the four-ply nylon suppressant and aluminum plate. This sytem was impacted at 45 degrees obliquity by a ball projectile at 2500 feet per second and 90 degrees yaw. In each of these tests, a single fragment was carried through the suppressant system, apparently as a cap on the projectile; otherwise, the suppressant functioned as efficiently as in previous tests. Selection of the spacer material for a floor area application of suppressant should obviously be based on a more extensive series of tests to find an optimum material in terms of areal density and weight-carrying ability.

Unclassified
Security Classification

DOCUMENT CONTROL DATA - R & D

(Security classification of title, body of abstract and indexing annotation must be entered when the overall report is classified)

1. ORIGINATING ACTIVITY (Corporate author) Denver Research Institute University of Denver Denver, Colorado	2a. REPORT SECURITY CLASSIFICATION Unclassified 2b. GROUP

3. REPORT TITLE
Reduction of Hazard From Secondary Fragments Created by Ballistic Penetration of Aircraft

4. DESCRIPTIVE NOTES (Type of report and inclusive dates)

5. AUTHOR(S) (First name, middle initial, last name)
R. F. Recht
W. G. Howell

6. REPORT DATE	7a. TOTAL NO. OF PAGES	7b. NO. OF REFS
October 1967	94	6

8a. CONTRACT OR GRANT NO.	9a. ORIGINATOR'S REPORT NUMBER(S)
DA 44-177-AMC-399(T) b. PROJECT NO. Task 1F121401A15003 c. d.	USAAVLABS Technical Report 67-49 9b. OTHER REPORT NO(S) (Any other numbers that may be assigned this report) 931-6702-F

10. DISTRIBUTION STATEMENT
This document has been approved for public release and sale; its distribution is unlimited.

11. SUPPLEMENTARY NOTES	12. SPONSORING MILITARY ACTIVITY
	U.S. Army Aviation Materiel Laboratories Fort Eustis, Virginia

13. ABSTRACT

The objective of this research effort was to establish a practical means of alleviating the hazard to personnel within occupied areas of Army aircraft due to secondary projectiles (spall and debris) created by ballistic impact of aircraft structure and equipment by small-arms projectiles. The characteristics of secondary fragments generated by ballistic penetration of typical aircraft structural materials were established for a variety of impact conditions. The impact conditions which created the greatest hazard to personnel due to secondary fragments were used to evaluate suppressant systems designed to reduce or eliminate this hazard. A suppressant system was developed which proved to be capable of stopping virtually all secondary fragments generated by impact of structural materials tested.

DD FORM 1 NOV 68 1473 REPLACES DD FORM 1473, 1 JAN 64, WHICH IS OBSOLETE FOR ARMY USE.

Unclassified
Security Classification

14. KEY WORDS	LINK A		LINK B		LINK C	
	ROLE	WT	ROLE	WT	ROLE	WT
vulnerability protection spall and debris, reduction of aircraft armor						